BOREAL ENVIRONMENT RESEARCH 13: 133–158
ISSN 1239-6095 (print) ISSN 1797-2469 (online)

Helsinki 28 April 2008

Optical properties of boreal lake waters in Finland and Estonia

Helgi Arst[1)], Ants Erm[2)], Antti Herlevi[3)5)], Tiit Kutser[1)], Matti Leppäranta[3)]*, Anu Reinart[4)] and Juhani Virta[3)]

[1)] *Estonian Marine Institute, University of Tartu, Mäealuse 10a, Tallinn 12618 Estonia*
[2)] *Marine Systems Institute, Tallinn Technical University, Akadeemia tee 21, 12618 Tallinn, Estonia*
[3)] *Department of Physical Sciences, P.O. Box 64, FI-00014 University of Helsinki, Finland (*corresponding author's e-mail: matti.lepparanta@helsinki.fi)*
[4)] *Tartu Observatory, 61602 Tõravere, Tartumaa, Estonia*
[5)] *Present address: GEO Secretariat, Case postale 2300, CH-2211 Geneva 2, Switzerland*

Received 23 Jan. 2007, accepted 1 Aug. 2007 (Editor in charge of this article: Timo Huttula)

Arst, H., Erm, A., Herlevi, A., Kutser, T., Leppäranta, M., Reinart, A. & Virta, J. 2008: Optical properties of boreal lake waters in Finland and Estonia. *Boreal Env. Res.* 13: 133–158.

A ten-year (1995–2005) research programme SUVI (Suomi–Viro) on the optics of Finnish and Estonian lakes has been completed. The objectives were to examine the light conditions, to map optically active substances (OAS), and to develop remote sensing methods. Altogether 14 Estonian and 7 Finnish lakes representing different types of water, from oligotrophic to hypertrophic and dystrophic were included. We performed extensive analyses of concentrations of three main OAS, light attenuation and Secchi depth. They varied among lakes and with seasons, but no systematic temporal change could be detected during the 10-year period. We studied the underwater light field using a spectrometer and two PAR quantum sensors, and elaborated three versions of optical classification of lake waters based on: (1) apparent optical properties and the amount of OAS, (2) irradiance reflectance spectra, and (3) light attenuation coefficient and the predominant OAS. We developed two models for determining the diffuse attenuation spectra of light, using data for (1) one wavelength and (2) three wavelengths, and elaborated a semiempirical model for quantitative description of the underwater light regime. We developed a bio-optical model for interpretation of remote sensing data that allows simulation of the reflectance spectra based on the concentrations of OAS. Winter expeditions were undertaken to examine the optical properties of ice and snow and the light conditions in the water beneath the ice cover. Gas pockets are the main optically active impurity in snow and ice. The transparency of ice is similar to that of lake water. The ice cover lowers the light level and makes the light more diffuse in the near surface liquid water layer.

Introduction

During the early 1990s, Estonian–Finnish collaboration in the research of coastal and inland waters increased remarkably. Optical investigations were taken as the main theme, leading to the signing in 1995 of an agreement on the SUVI (Suomi–Viro) programme between the Department of Geophysics of the University of Helsinki and the Estonian Marine Institute. A pilot

study had been performed in 1994. This topic was highly stimulating, because optical research on natural waters was progressing from clear ocean waters to include multicomponental turbid waters. The SUVI programme lasted 10 years, producing a vast amount of data on optics and optically active substances (OAS) of 21 Estonian and Finnish lakes over a 10-year period and resulted in three Ph.D. theses (Kutser 1997, Reinart 2000, Herlevi 2002a), two M.Sc. theses (Sipelgas 2002, Lehmusjärvi 2004) in Tartu and Helsinki and about 40 peer-reviewed articles. SUVI seminars were also arranged annually during 1995–2003 in both countries.

The objectives of SUVI were to examine the light conditions in Finnish and Estonian lakes, map OAS in lake waters and to develop remote sensing methods for mapping the ecological conditions in lake waters. The study lakes represented different types of water, from oligotrophic to hypertrophic and dystrophic. The fieldwork was done first in summer, but winter expeditions have also been undertaken in January–April since 2000 when ice and snow cover on lakes is present. The data include profiles of underwater spectral irradiance, light attenuation and absorption, remote-sensing reflectance spectra, light transmission through snow and ice, and concentrations of three OAS (coloured dissolved organic matter, suspended matter and chlorophyll *a*). The data programme was in all successful, and the 10-year database produced provides a unique time slice — 'year 2000 situation' — of the optical state of Finnish and Estonian lake waters for comparison with past and future data.

This paper presents the final results of the SUVI programme.

Measurement programme

Study sites

In the ice-free period (1994–2005) SUVI sites included 14 Estonian and 7 Finnish lakes, and the winter expeditions (2000–2005) covered 11 Estonian and 3 Finnish lakes (Fig. 1). Additionally one brackish water basin, Santala Bay in the Gulf of Finland, was examined during the winter expeditions. The trophic type and main morphometric data of the SUVI water bodies are shown in Table 1.

The number of summer measurements (N_s, Table 1) indicated the series when all three OAS — chlorophyll *a*, suspended matter and coloured dissolved organic matter (CDOM) — were studied, and when the spectrometric data processing of the water samples was performed. When one of these parameters was missing, we did not include the corresponding measurement series in our database. Note that N_s describes all types of series including water samples from different depths at the same sampling station or measurements at several stations. The number of underwater irradiance measurements and Secchi disk data is smaller than the value of N_s shown in Table 1.

During the winter expeditions one brackish water basin, Santala Bay, on the northern coast of the Gulf of Finland was also examined (about 30 measurement series). This was desirable for comparisons because brackish water ice is structurally different from lake ice, and therefore the optical properties of the ice as well as the light conditions beneath the ice are different. At this site, the water body is oligotrophic/mesotrophic, the mean depth is 5 m, the surface water salinity is about 5‰, and the resulting ice salinity is 1‰–2‰.

Laboratory measurements

Laboratory measurements of the water samples collected were carried out. In summer these samples were often taken from different depths at each site, and in winter we analysed not only the under-ice water, but also the ice and snow meltwater.

We determined the concentration of chlorophyll *a* (C_{chl}, mg m^{-3}) using the method of Lorenzen (1967). The concentration of total suspended matter (C_s, mg l^{-1}) was determined by its dry weight after filtration of the water through polycarbonate membrane filters.

'Spectrometric' attenuation coefficients of light were determined from unfiltered ($c^*(\lambda)$) and filtered ($c_f^*(\lambda)$) water samples, where λ is wavelength, in the spectral band 350–700 nm (Arst 2003). They were obtained as the difference $c(\lambda) - c_d(\lambda)$, where $c(\lambda)$ and $c_d(\lambda)$ are the

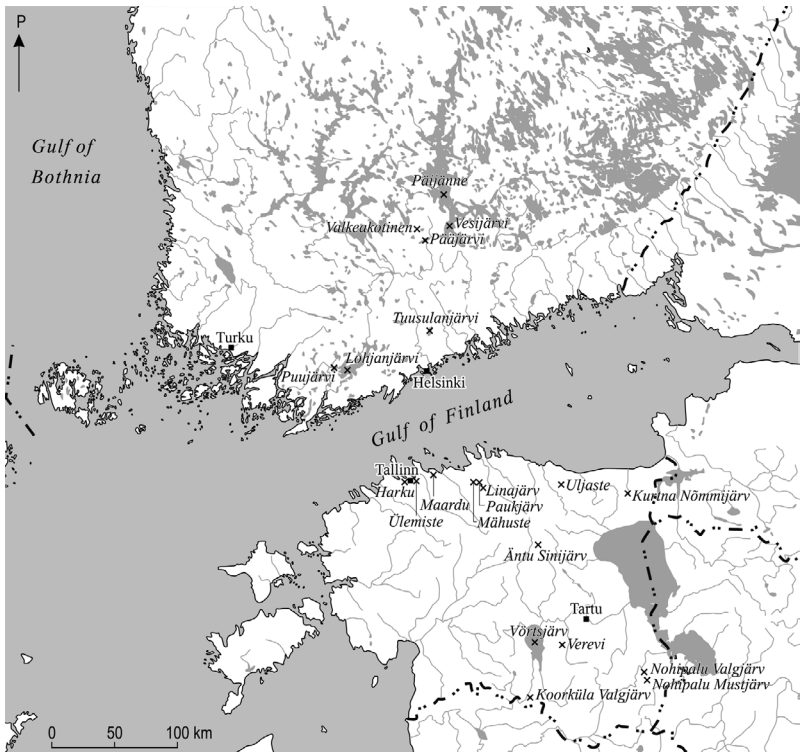

Fig. 1. A map of Estonia and southern Finland showing the study lakes.

Table 1. Measurements of bio-optical characteristics in Estonian (E) and Finnish (F) lakes between 1994 and 2005. The *N* columns show the number of summer field trips (N_t), the number of summer measurement series (N_s) and the number of winter expeditions (N_{ice}).

Lake	Limnological type	Area (km^2)	Average depth (m)	Observation period	N_t (N_s)	N_{ice}
Äntu Sinijärv (E)	Alkalitrophic	0.024	3.5	1994–2005	5 (5)	3
Päijänne (F)	Oligotrophic	1038	15.9	1996–2002	11 (22)	–
Puujärvi (F)	Oligotrophic	7	6	1997	3 (7)	–
Koorküla Valgjärv (E)	Oligotr/mesotroph	0.441	8.5	1997–2001	9 (32)	–
Paukjärv(E)	Oligotrophic	0.086	5	1999–2002	17 (54)	2
Kurtna Nõmmjärv (E)	Dyseutrophic	0.156	3.1	1995–1996	5 (6)	–
Nohipalu Valgjärv (E)	Oligotr/mesotroph	0.063	6.2	1994–2001	19 (36)	3
Maardu (E)	Dyseutrophic	1.75	2.5	1999–2003	25 (49)	5
Vesijärvi (F)	Eutrophic	112	6.6	1994–2002	12 (30)	–
Uljaste (E)	Semidystrophic	0.63	2.2	1995–1996	8 (9)	–
Mähuste (E)	Oligotr/mesotroph	0.057	3.7	2001–2005	8 (31)	3
Pääjärvi (F)	Mesotr/mesohumic	13.4	14.4	1994–2005	13 (29)	3
Linajärv (E)	Semidystrophic	0.058	3.8	1999–2000	7 (26)	–
Lohjanjärvi (F)	Eutrophic	94	15	1997–2002	7 (32)	–
Verevi (E)	Hypertrophic	0.126	3.6	1994–2002	17 (43)	2
Valkeakotinen (F)	Dystrophic	0.036	3.0	1995	2 (2)	2
Tuusulanjärvi (F)	Hypertrophic	6.1	3.1	1996–2002	15 (21)	–
Ülemiste (E)	Hypertrophic	9.6	2.5	1997–2002	48 (247)	6
Võrtsjärv (E)	Eutrophic	270	2.8	1994–2005	25 (58)	2
Nohipalu Mustjärv (E)	Dystrophic	0.219	3.9	1995–2003	14 (14)	2
Harku (E)	Hypertrophic	1.64	2	1999–2002	28 (50)	3

beam attenuation coefficients for natural and distilled water, respectively. These measurements were made at a spectral intervals of 10 nm in the PAR (photosynthetically active radiation) band, 400–700 nm. The term 'spectrometric attenuation coefficient' needs explanation. As known (Zaneveld *et al*. 1992, Bricaud *et al*. 1995b), the experimental determination of the true values of the beam attenuation coefficient (c) is complicated. Theoretically, the beam transmittance should contain no contribution from scattered light, but in reality small-angle forward scattering does reach the detector. The measured transmittance then exceeds the theoretical value and the attenuation coefficient determined from the measured transmittance is smaller than the true value. Actually, the direct spectrophotometer reading, $c^*(\lambda)$, is the following:

$$c^*(\lambda) = c(\lambda) - Fb(\lambda) - c_d(\lambda) \quad (1)$$

where $b(\lambda)$ is the light-scattering coefficient and F is a coefficient showing the contribution of small-angle forward scattering to the radiation measured by the spectrophotometer. Equation 1 is also valid for filtered water but the term $Fb(\lambda)$ is considerably smaller due to the decrease in scattering after filtration. We performed our laboratory measurements with a commercial Hitachi U1000 spectrophotometer. Unfortunately, the value of F for this instrument is not known and therefore we refer to the measurement result not as a 'beam attenuation coefficient', but as a 'spectrometric' attenuation coefficient. We found (Arst *et al*. 1996, 1999a, 1999b) that although $c^*(\lambda)$ differs from the true beam attenuation coefficient, the averaged value over the PAR band, c^*_{PAR}, can be used for characterizing the optical quality and transparency of water at different depths.

The light attenuation coefficient of CDOM can be considered as the sum of the absorption coefficients of CDOM ($a_{CDOM}(\lambda)$) and the scattering/absorption coefficients of colloids (extremely small particles penetrated through the filter). The contribution of colloids is small in comparison with the total attenuation coefficient of light for CDOM (Bricaud *et al*. 1981, Davies-Colley and Vant 1987). Additionally, the dissolved matter also contains an optically non-active fraction. For filtered water $b(\lambda)$ is small and $c^*_f(\lambda)$ can be considered approximately equal to $a_{CDOM}(\lambda)$ in the water. We carried out a special study to estimate the difference between $c^*_f(\lambda)$ and $a_{CDOM}(\lambda)$ in lake waters (Sipelgas *et al*. 2003). Since chemical analytic techniques for determining the compounds of CDOM are difficult, the amount of CDOM is usually described with the value of c^*_f (or a_{CDOM}) in some reference wavelength λ_0. Here this is taken as λ_0 = 380 nm, and so our database contains the values of c^*_f(380 nm).

Ice samples were processed for thick and thin sections in a coldroom. The thick sections show the stratigraphy and gas bubbles in the ice when examined on a dark background in normal light, while the thin sections examined between crossed polarized sheets provide the size and shape of the ice crystals (e.g. Leppäranta and Kosloff 2000). To determine the concentrations of impurities in the ice, the samples were melted and the meltwater was analysed in the same way as the normal water samples (Leppäranta *et al*. 2003b).

Field measurements

Water transparency is expressed as a Secchi depth, i.e. the depth where the Secchi disk is just visible (z_{SD}).

The vertical profiles of the beam attenuation and absorption coefficients in the water body were detemined at nine wavebands using an ac-9 instrument (WET Labs Inc., Philomath, Oregon, U.S.A.) (Herlevi *et al*. 1999, Herlevi 2002a, 2002b). This is a spectral absorption/attenuation meter that uses nine band-pass filters in different spectral channels. In 1997–1999 the central wavelengths of these channels were 412, 440, 488, 510, 532, 555, 650, 676 and 715 nm (in early 2000 channel 532 nm was replaced by a 630-nm channel).

The spectral downwelling irradiance ($E_d(z)$, W m^{-2} nm^{-1}) was profiled in the water column using the LI-1800 UW spectroradiometer (LI-COR Corporation, Lincoln, Nebraska, U.S.A.). This instrument measures the irradiance spectra over 300–1100 nm in air and 350–850 nm in water with a spectral resolution of 2 nm. The description of this instrument as well as the

measurement methods used is given by Virta and Herlevi (1999) and Herlevi (2002b).

The quantum irradiance (q_{PAR}, μmol m^{-2} s^{-1}) was measured as integrated over the PAR band, including downwellling planar irradiances in air and water and also scalar irradiance (only in water). The LI-192 SA and LI-193 SA instruments (LI-COR) were used.

Optical remote-sensing measurements were carried out from boats in eight Estonian and five Finnish lakes. The Pegasus telespectrometer and later (since 1998) the ST1000 instrument (designed by Ocean Optics Inc., Dunedin, Florida, USA) were used. Pegasus (Arst *et al.* 1997a) was a mechanically scanning instrument that allowed measurement of the upwelling nadir radiance ($L_u(\lambda)$), downwelling irradiance ($E_d(\lambda)$) and downwelling zenith radiance ($L_d(\lambda)$) above the water surface in the visible part of the spectrum (375–720 nm). The spectral resolution of the instrument was 6–8 nm. The ST1000 had three charge-coupled device (CCD) sensors to measure the same parameters as Pegasus with a spectral interval of 0.5 nm. The instrument was designed for laboratory measurements, but was rebuilt for field conditions at the Estonian Marine Institute as described in Kutser *et al.* (1999).

During winter expeditions, the thicknesses of ice and snow were recorded, and the state of the surface was described and photographed. Water and ice samples were also collected. The ice provides a stable platform for performing these measurements. For irradiance measurements under the ice cover, a special device was constructed in Estonia (Leppäranta *et al.* 2003a, Arst *et al.* 2006). This device allowed taking of records at a distance of about 1 m from the ice hole in the horizontal direction and at different depths under the ice down to 2.25 m. Two PAR sensors were used in this system: the LI-192 SA and LI-193 SA, the first for measuring the quantum planar irradiance, the second for the quantum scalar irradiance. LI-COR 1800UW measurements were also taken using a long arm to install the sensor 2–3 m away from the deployment opening in the ice. To examine the role played by snow, measurements were also taken with snow removed from the site. The values of albedo were determined with two additional LI-192 SA sensors: one for measuring the incident quantum irradiance and the second for the backscattering from the snow or ice cover. In the field we first measured the underwater irradiance profile of snow-covered ice sheet and then the snow was removed from the area to a radius of 2 m. Thus, the albedos both of the snow and the ice were recorded. The ice samples were later photographed in natural light and sometimes also in polarized light (in the laboratory). The ice samples were melted (the whole sample and distinctive layers separately) and the same parameters were measured for the meltwater as for the normal water samples.

Additional site data included the weather conditions, especially under cloudy sky. In many cases conductivity-temperature-depth (CTD) profiles were also taken.

Parameters derived from the data

Relying on the $c^*(\lambda)$ values measured, we calculated average values over the PAR region (c^*_{PAR}). We determined the contribution to scattering by colloids in $c^*_f(\lambda)$ spectra and then estimated the respective values of $a_{CDOM}(\lambda)$.

One of the parameters widely used in the optics of water bodies is the irradiance attenuation coefficient $K_d(z,\lambda)$, commonly called the 'diffuse attenuation coefficient' (Preisendorfer 1961, Jerlov 1976, Dera 1992, Kirk 1996, Arst 2003). The basic equation that determines $K_d(z,\lambda)$ is

$$K_d(z,\lambda) = -\frac{1}{E_d(z,\lambda)}\frac{dE_d(z,\lambda)}{dz} \qquad (2)$$

Quantum irradiance, $q_d(z,\lambda)$, can be used in Eq. 2 instead of $E_d(z,\lambda)$.

In thin homogeneous water layers from depths z_1 to z_2, the diffuse attenuation coefficient is constant (the wavelength argument is ignored for brevity):

$$K_d([z_1, z_2]) = -\frac{1}{z_2 - z_1}\ln\left[\frac{q_d(z_2)}{q_d(z_1)}\right] \qquad (3)$$

When K_d in some layer is not constant, Eq. 3 still gives an 'effective' attenuation coefficient since it represents the rate at which the radiation is reduced with depth. Thus, when no data are available on the change in irradiance inside the layer of a medium, we can determine the

effective attenuation coefficient by measuring the irradiances on the upper and lower surfaces of the layer. For an entire water body or for an extensive water layer, a representative value of K_d is usually determined, based on irradiance data at different depths, by performing linear regression analysis on a semilogarithmic depth-irradiance coordinate system (Dera 1992, Reinart 2000, Arst 2003). In this way we determined the values of diffuse attenuation coefficient for the PAR region ($K_{d,PAR}$), using the vertical profiles of $q_{d,PAR}(z)$ in the water.

Surface reflectance (r) plays a crucial role in winter conditions when the ice and snow optics are examined. Irradiances are measured above and below the ice sheet, and reflectance must be taken into account to determine the attenuation. In the ice cover the attenuation coefficient is vertically not constant since there are sublayers of differing optical properties, including snow, snow-ice and congelation ice as well as the gas bubbles.

The effective attenuation of light in the ice cover ($K_{d,i}$) can be approximately described by an equation similar to Eq. 3:

$$K_{d,i}\left(D_i\right) = -\frac{1}{D_i}\ln\left[\frac{q_d\left(D_i\right)}{\left(1-r\right)q_d\left(0^+\right)}\right] \quad (4)$$

Here D_i is the thickness of the ice cover, r is the reflectance and $q_d(0^+)$ is incident solar irradiance on the upper ice surface. Although the values of $K_{d,i}$ calculated with Eq. 4 cannot describe the variation in optical properties inside the ice layer, they do allow us to compare the light attenuation properties of the ice cover in different lakes.

Note that although Eqs. 2–4 describe the attenuation of spectral irradiance, the corresponding exponential law is also widely used for calculating the values of integral underwater irradiance, using the average PAR region values for $K_{d,PAR}$. The accuracy of this approach for ice-free water bodies was estimated in Arst *et al.* (2000).

The reflectance of the ice/snow cover was calculated as the ratio of upwelling irradiance to downwelling irradiance:

$$r_i = \frac{q_u\left(z = 0^+\right)}{q_d\left(z = 0^+\right)} \quad (5)$$

where the subscripts 'd' and 'u' are for downwelling and upwelling irradiance, respectively, and the 0^+ refers to the region just above the surface.

We calculated the ratio of quantum planar irradiance to the corresponding scalar irradiance ($q_{d,PAR}/q_{0,PAR}$) at different depths in the water. This ratio gives information on the directional distribution of the underwater radiance. The scalar irradiance includes both the downwelling and upwelling light and represents all angular directions equally. The downwelling planar irradiance, in accordance with the cosine law, is progressively less affected by light flux as its zenith angle increases (Kirk 1996).

The main remote-sensing characteristics derived from the measurement data were remote sensing reflectance $r(\lambda)$ and the diffuse component of water reflectance ($r_D(\lambda)$). The first parameter was calculated as follows:

$$r\left(\lambda\right) = \frac{L_u\left(\lambda\right)}{E_d\left(\lambda\right)} \quad (6)$$

We measured the full spectra of these characteristics. However, for interpretation of the data obtained (i.e. associating their values with the amount of various OAS in the water) several methods area available, using the results for only a few wavelengths or for the entire spectrum. When we measure $L_u(\lambda)$ and simultaneously $L_z(\lambda)$, we can estimate the diffuse (or water-leaving) component of reflectance, assuming that from the surface it reflects 2% of $L_z(\lambda)$. Then $r_D(\lambda)$ can be calculated:

$$r_D\left(\lambda\right) = \frac{0.02L_z\left(\lambda\right)}{E_d\left(\lambda\right)} \quad (7)$$

However, the results obtained with Eq. 7 can be considered only as approximate: during sunny days and with wind speeds more than 5–7 m s^{-1}, Eq. 7 can bring about remarkable errors (Arst 2003). The suitability of this approach is also dependent on the solar altitude (maximal errors will occur when the sun is near the zenith) and measurement direction.

Results

Many papers were published during the 10-year period of SUVI. In fact, the SUVI materials

(measurement programme, data, analysis, model calculations, etc.) are so voluminous that it is impossible to describe them in one paper. Thus here, we shall present mainly selected results which have not been published earlier as well as the general conclusions.

Inherent optical properties of the water and concentrations of OAS determined from water samples

Profound analyses of the dataset containing the concentrations of three main OAS and c^*_{PAR} for 885 measurement series obtained between 1992 and 2002 in 23 Estonian and 7 Finnish lakes and some regions of the Baltic Sea (135 'sea series') are presented in Arst (2003). For 428 sampling stations we also had the Secchi disk data and the relationships between z_{SD} and other parameters. The minimum, maximum and median values of OAS and c^*_{PAR} for each lake are also presented in Arst (2003). However, nine Estonian lakes were studied in 1992–1993, i.e. these lakes cannot be considered in connection with the SUVI project. On the other hand, during 2003–2005 we performed additional measurements in some SUVI lakes. Thus, we repeated the correlation analysis using the SUVI dataset, considering the associations between $K_{d,PAR}$ and other parameters, which was not done by Arst (2003) or presented in our earlier publications (Arst *et al.* 1996, Mäekivi and Arst 1996, Arst *et al.* 1998, Nõges *et al.* 1998, Reinart *et al.* 1998a, Arst *et al.* 1999a, 1999b, Reinart and Herlevi 1999, Erm *et al.* 2002, Sipelgas *et al.* 2003, Reinart *et al.* 2005). In the present paper we firstly show the average values of c^*_{PAR}, C_{chl}, C_s, c^*_f(380 nm) and z_{SD} for each SUVI lake (Table 2).

The analysis of the complete SUVI dataset shows that the values of OAS, c^*_{PAR}, $K_{d,PAR}$ and z_{SD} vary essentially among lakes and also with the seasons, which was expected since we considered very different types of lakes. One example is the clear-water Äntu Sinijärv: since the bottom was visible, the Secchi disk data were obtained using horizontal measurements. The approximate value of z_D for Äntu Sinijärv is 13 m; note that in the other lakes the maximum reading for z_D was 7 m (maximum average was 5.5 m). Special attention should be focused on the last two lakes Nohipalu Mustjärv and Harku, both of which are rather extreme, but for different reasons. The high values of c^*_{PAR} in dystrophic Nohipalu Mustjärv are caused mainly by very high concentration of CDOM (maximum measured value of c^*_f(380 nm) was 85 m^{-1}). In Harku we can observe the extraordinarily high averaged values of c^*_{PAR}, C_{chl} and C_s (maxima 50 m^{-1}, 409 mg m^{-3} and 96 mg l^{-1}, respectively) and the very small values of z_{SD} (minimum 0.1 m).

Temporal variations and correlations of bio-optical properties were studied based on repeated measurements in four Estonian lakes (Paukjärv, Ülemiste, Maardu and Harku) during 1999–2001. A special investigation was performed for Ülemiste (a drinking-water basin for the City of Tallinn), measuring the parameters at five sampling stations from 1997 to 2001. The results of these studies are published in Erm *et al.* (1999, 2001, 2002) and Reinart *et al.* (2001). It is worthwhile to study the possible long-term changes in the bio-optical parameters in SUVI lakes. However we have only five lakes in which the observation period is 7 years or more (*see* Table 1). Temporal changes in three parameters, C_{chl}, c^*_f(380 nm) and z_{SD} for Pääjärvi, Vesijärvi, N. Valgjärv and Võrtsjärv are shown in Fig. 2. The concentration of CDOM and the value of z_D showed practically no long-term trend in all four lakes (only in Võrtsjärv in 2005 were somewhat higher values of c^*_f(380 nm) than in 1994–2004). In two Finnish lakes (Pääjärvi and Vesijärvi) the chlorophyll content appeared to increase with time, while in N. Valgjärv and Võrtsjärv seasonal variations predominated.

As is known, the value of c^*_{PAR} is formed under the influence of all three OAS. Consequently, it is of interest to determine the multiple regression of c^*_{PAR} *vs.* (C_s, C_{chl}, c^*_f(380 nm)). The SUVI dataset gave us the following regression formula:

$$c^*_{PAR} = 0.406C_s + 0.0522C_{chl} + 0.194c^*_f(380\ \text{nm}), \quad (8)$$

where $R^2 = 0.962$, $N = 801$, SD = 2.15 m^{-1} and the $p < 0.000001$. Comparison of the measured and calculated (with Eq. 8) values of c^*_{PAR} is presented in Fig. 3. This type of relationship can

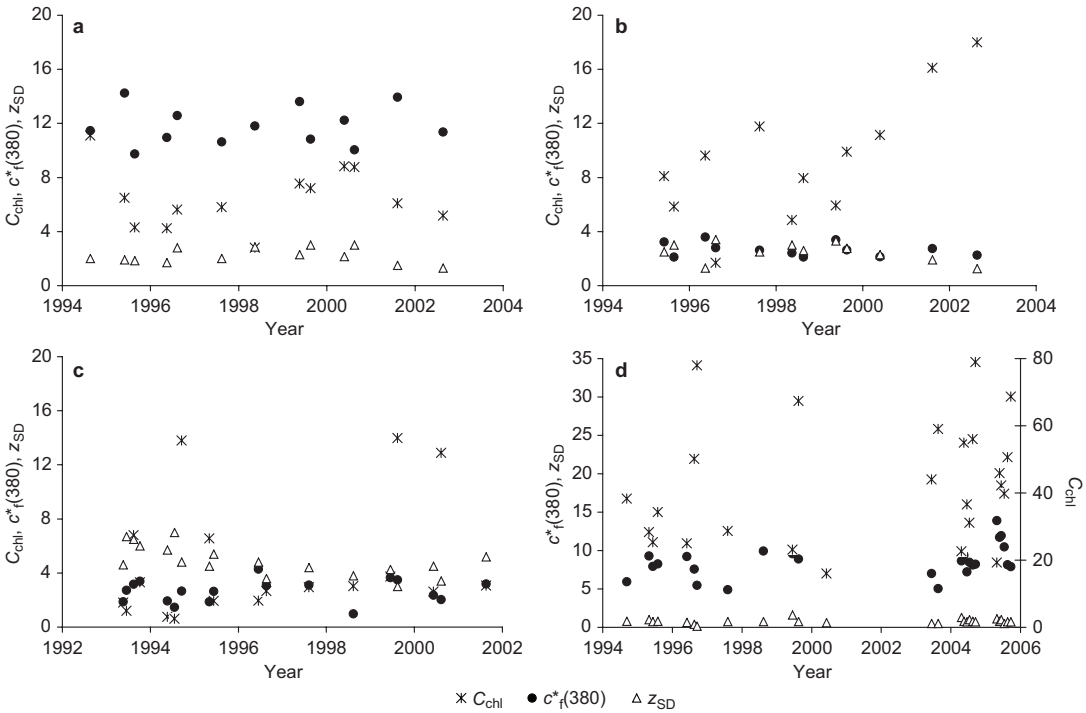

Fig. 2. Temporal variations in chlorophyll *a* (C_{chl}, mg m^{-3}), Secchi depth (z_{SD}, m) and CDOM ($c^*_f(380)$, m^{-1}) in (**a**) Lammi Pääjärvi, (**b**) Vesijärvi, (**c**) Nohipalu Valgjärv and (**d**) Võrtsjärv.

Table 2. Average values of light attenuation coefficient c^*_{PAR}, chlorophyll content C_{chl}, concentration of suspended matter C_s, light attenuation coefficient for filtered water at 380 nm, $c^*_f(380$ nm), and Secchi depth z_{SD} obtained from the SUVI dataset for various lakes.

Lake	c^*_{PAR} (m^{-1})	C_{chl} (mg m^{-3})	C_s (mg l^{-1})	$c^*_f(380$ nm) (m^{-1})	z_{SD} (m)
Äntu Sinijärv (E)	0.5	0.56	2.9	1.5	13
Päijänne (F)	1.2	2.7	1.1	4	5.5
Paukjärv(E)	1.2	5.4	2.1	1.3	5.2
Puujärvi (F)	1.3	3.8	1.3	2.6	4
Koorküla Valgjärv (E)	1.6	9.9	2.5	2.3	4
N. Valgjärv (E)	1.9	13	3.3	3.5	4.9
Kurtna Nõmmjärv (E)	2.2	2.2	3.7	5	3.6
Maardu (E)	2.4	12	4.1	5.3	2.5
Vesijärvi (F)	2.5	10.7	3.9	2.9	2.5
Mähuste (E)	2.9	23	2.6	6.9	2.7
Uljaste (E)	3.1	14.7	6.7	6.6	2.3
Pääjärvi (F)	3.2	6.4	4.5	11.2	1.8
Linajärv (E)	4.4	21	4.5	10.6	1.7
Lohjanjärvi (F)	5.2	14.2	6.7	9.3	1.3
Verevi (E)	6.5	40	8.7	6	2.2
Valkeakotinen (F)	6.3	8.1	6.5	16.6	1
Tuusulanjärvi (F)	10.6	27	18.5	10.3	0.65
Ülemiste (E)	10.9	46	15.9	6.8	0.75
Võrtsjärv (E)	11.7	45	17.8	8.3	0.8
Nohipalu Mustjärv (E)	15.9	15.2	6.4	65	0.5
Harku (E)	28	156	42	12.1	0.35

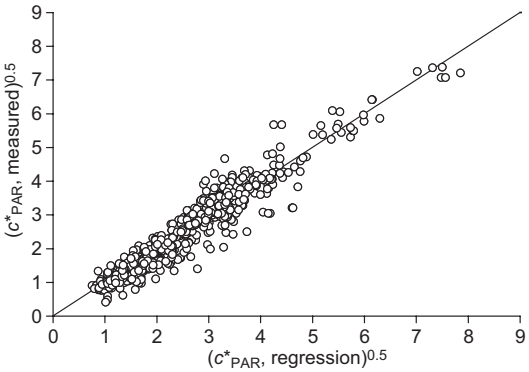

Fig. 3. Values of $(c^*_{PAR})^{0.5}$ (c^*_{PAR} in m^{-1}) obtained from measurements and from regression formulae (Eq. 8).

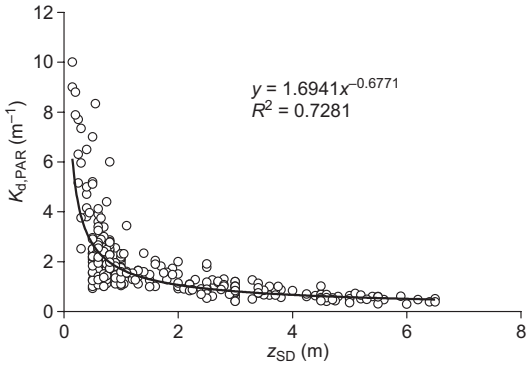

Fig. 4. Regression curve of the relationship $K_{d,PAR}$ *vs.* z_{SD} obtained from SUVI dataset ($N = 267$)

be used in practice when one wants to determine a variable when three others are known.

Arst (2003) obtained a regression formula similar to Eq. 8 using the previously mentioned database (altogether 885 series, the SUVI lake data obtained in 1994–2002 and the results for Estonian small lakes and the Baltic Sea obtained in 1992–1993):

$$c^*_{PAR} = 0.336C_s + 0.0506C_{chl} + 0.196c^*_f(380\ nm). \quad (9)$$

The constants of these two formulae differ slightly, but the determination coefficient was the same. It shows that this type of formula is suitable for different datasets, although the coefficients may vary.

There are three variables, all describing the transparency (or turbidity) of the water body: z_{SD}, c^*_{PAR} and $K_{d,PAR}$ (the type of a lake can be characterized also by its colour). The correlations $K_{d,PAR}$ *vs.* z_{SD} and $K_{d,PAR}$ *vs.* c^*_{PAR} are shown in Figs. 4 and 5. The power function regression gives a rather high value for the determination coefficient: 0.723 (Fig. 4). However, for high values of $K_{d,PAR}$, Secchi depth (z_D) is unable to describe any changes in $K_{d,PAR}$, although for small values of $K_{d,PAR}$ Secchi depth is a suitable characteristic for describing water transparency. Note that Arst (2003) concluded similarly regarding the relationship c^*_{PAR} *vs.* z_{SD}. The regression between inherent (c^*_{PAR}) and apparent ($K_{d,PAR}$) optical properties is linear, but the value of R^2 is not very

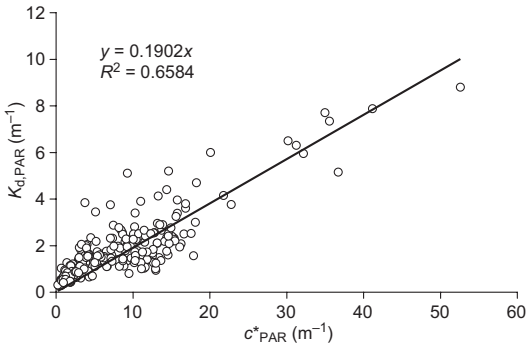

Fig. 5. Regression $K_{d,PAR}$ *vs.* c^*_{PAR} obtained from SUVI dataset ($N = 272$).

high, possibly due to the fact that in very turbid water the irradiance attenuates very quickly with depth, which can bring about substantial errors in $K_{d,PAR}$ (Fig. 5).

The correlations between transparency (or turbidity) characteristics and the different OAS are presented in numerous publications (Arst *et al*. 1996, 1999a, Arst 2003, Erm *et al*. 1999, 2001, 2002). An interesting result is that in determining the regression formulas separately for each lake (the parameters changed due to seasonal variability), we can obtain rather different constants for these formulas, which is caused by the concrete bio-optical type of lake. Based on data with a large variation range (many lakes together), true algorithms that describe the relationships between water properties can be derived (Erm *et al*. 2002, Arst 2003).

Inherent optical properties measured *in situ* (instrument ac-9)

During SUVI, repeated *in situ* measurements of the inherent properties of lakes were carried out using a WetLabs instrument ac-9 (Herlevi *et al*. 1999, Herlevi 2002a, 2002b). The ac-9 is a spectral absorption/attenuation meter that uses nine band-pass filters in different spectral channels. It performs simultaneous measurements of the beam attenuation (c) and absorption (a) coefficients in the water by incorporating a dual-path optical configuration in a single instrument. Based on these data, it was also possible to calculate the scattering coefficient (b) using the formula: $b = c - a$. The accuracy of the ac-9 is ±0.005 m^{-1} (Herlevi 2002a, 2002b). The ac-9 measurements were performed as depth profiles in seven Finnish and six Estonian lakes in 1997–2000 (Herlevi *et al*. 1999, Herlevi 2002a, 2002b. The results obtained were thoroughly analysed by Herlevi (1999, 2002a, 2002b). Comparison of the spectra of the attenuation, absorption and scattering coefficients were carried out, dividing the lakes in two groups: turbid and clear-water. The diurnal variation and vertical change were studied. Special attention was focused on parameterization of the spectral curve of the scattering coefficient. In the generally used form (λ_0 is some reference wavelength)

$$b(\lambda) = b(\lambda_0)\left(\frac{\lambda_0}{\lambda}\right)^{p_b} \quad (10)$$

The exponent p_b is close to 1, but with marked variations from 0.13 to 2.42 (Herlevi 2002b). We tried to estimate the associations between the values of p_b and the concentrations of the OAS (Paavel *et al*. 2007). We were unsuccessful in finding a good correlation between p_b and the concentration of any single OAS, although multiple regression between p_b and three OAS jointly can give rather high determination coefficients. To predict this slope, in the analysis we used the multiple linear regression module of STATISTICA 6.0 (StatSoft Inc. 2001) including the measured OAS values as well as their pairwise products ($C_{chl} \times C_s$, $C_{chl} \times c^*_f(380\ nm)$ and $C_s \times c^*_f(380\ nm)$). Forward stepwise method was applied to select the best fitting model. The regression formula obtained is the following:

$$p_b = 0.7964 + 0.00964C_s \times c^*_f(380\ nm) - 0.0453C_s - 0.0124C_{chl} \quad (11)$$

The units of C_s, C_{chl}, and c^*_f are mg l^{-1}, mg m^{-3} and m^{-1}, respectively. The statistical parameters of this regression were: $N = 73$, $R^2 = 0.668$, R^2 (adjusted) = 0.655, SD of estimate = 0.259, $p < 0.000001$.

However, for five Finnish lakes (Pääjärvi, Lohjanjärvi, Päijänne, Tuusulanjärvi and Vesijärvi) together, simple linear multiple regression also resulted in a high value of $R^2 = 0.764$ (Fig. 6). The corresponding regression formula was

$$p_b = 0.0492C_s - 0.0306C_{chl} + 0.0922c^*_f(380\ nm) + 0.212 \quad (12)$$

where $N = 41$, SD = 0.27 and $p < 0.000001$.

In three Finnish and two Estonian lakes, the values of p_b in May–June exceeded markedly those in August. In Vesijärvi, Koorküla Valgjärv and Ülemiste the differences were about 20%–40%, while for Lohjanjärvi and Tuusulanjärvi they were more than 50%. Gallegos *et al*. (2005) also found a seasonal trend for p_b characterized by relatively high values in early spring and declines during the summer bloom. The reason why the wavelength dependence of the scattering coefficient is larger in spring than in late summer could be the different sizes and types of particles in the water.

Underwater irradiance and light attenuation coefficients determined using LI-1800, LI-192SA and LI-193SA sensors. Model calculations.

Measurements of underwater irradiance

During 1995–2005 we performed a total of 132 spectral measurement cycles in the SUVI lakes (the LI-1800 UW instrument was used). Each cycle comprised four series of downwelling (E_d) and four series of upwelling (E_u) irradiance at various depths. E_d was measured lowering the instrument to depths of 0.5 m, 1 m, 1.5 m, etc., until there was just enough light for obtaining reasonable data. E_u was measured after turning device face down at the same depths; no

instrument shading corrections were made to the measurements. The final result was obtained averaging the data of four series at each depth. PAR irradiances were integrated from the spectral data:

$$E_{d,PAR}(z) = \int_{400}^{700} E_d(\lambda, z)\, d\lambda \qquad (13)$$

For determining the depth-averaged values of the attenuation coefficient from spectral ($K_d(\lambda)$) and PAR data ($K_{d,PAR}$, $K_{0,PAR}$), a similar method was used for both cases: irradiance values at all depths were fitted by least-squares to a straight line on a semilog plot, the slope of which gives $K_d(\lambda)$. If necessary, additional smoothing by moving averages over 6-nm intervals was done. To make the results from different devices comparable, mostly the values of K_d for the 0.5–2-m layer were used. Only for very high attenuation (irradiance values beyond the sensitivity limit) was a thinner layer used.

Measurements were carried out twice per year, in May or June and in August, mostly around noon (to avoid changes in K_d due to different solar zenith angles). For a summarized overview the measurements carried out in ten Estonian lakes (Nohipalu Mustjärv and Valgjärv, Võrtsjärv, Ülemiste, Uljaste, Verevi, Kurtna Nõmmjärv, Koorküla Valgjärv, Paukjärv, Äntu Sinijärv) and five Finnish lakes (Valkeakotinen, Tuusulanjärvi, Pääjärvi, Päijänne, Vesijärvi) were used. In selecting the lakes we took into account the representativeness of ecosystems

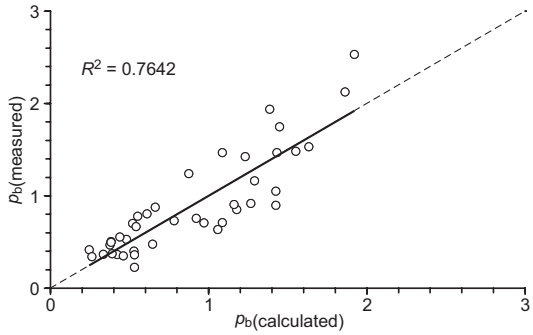

Fig. 6. Comparison of p_b(measured) and p_b(calculated) calculated with Eq. 14 (only the data of Päijänne, Vesijärvi, Lammi Pääjärvi, Lohjanjärvi and Tuusulanjärvi were used; N = 41).

(ranging from oligotrophic to hypertrophic) and the water constituent concentrations to cover the variability in lake characteristics for our region (Table 1).

Typical results for the irradiance measurements in various lakes are shown in Fig. 7. The most striking feature of the observations in many Estonian and Finnish lakes is the very rapid attenuation of irradiance with depth in the region of 400–500 nm, which generally leads already to small values of irradiance in this waveband at depths exceeding 1.5–2 m. The reason is strong absorption by CDOM. Irradiance also diminishes rapidly at the red end of the spectrum due to absorption by water itself, although not to the same extent as at the blue end. The wavelength of maximal penetrating radiation (λ_{max}) is around

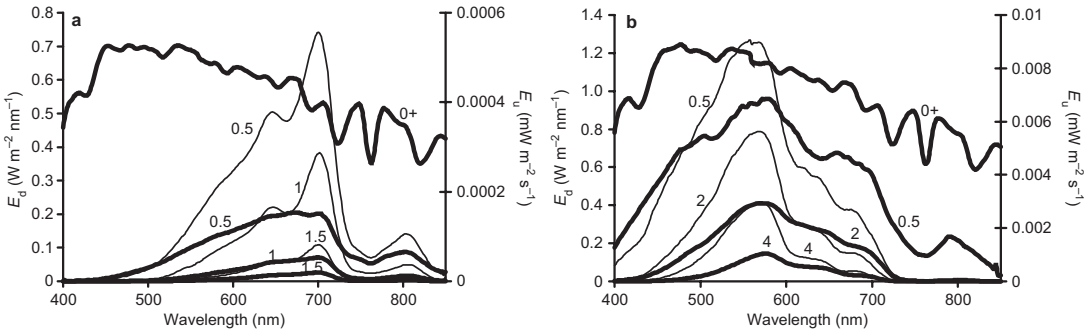

Fig. 7. Spectral distribution of underwater irradiance in different lakes: (**a**) Valkeakotinen (23 August 1995), and (**b**) Vesijärvi (1 June 1995). Thick lines represent the incident (0+) and underwater downward irradiance (E_d), thin lines represent upward irradiance (E_u). Depth in m is shown near each curve. Note that the scale of E_u is in mW m^{-2} s^{-1}, i.e. 10^{-3} the scale of E_d.

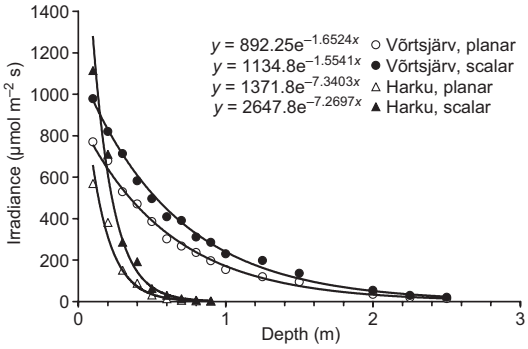

Fig. 8. Two examples (Võrtsjärv 27 April 2005, and Harku 16 June 2005) of the vertical profiles of quantum irradiance in the PAR band of spectrum, measured with the LI-192 SA (planar) and LI-193 SA (scalar).

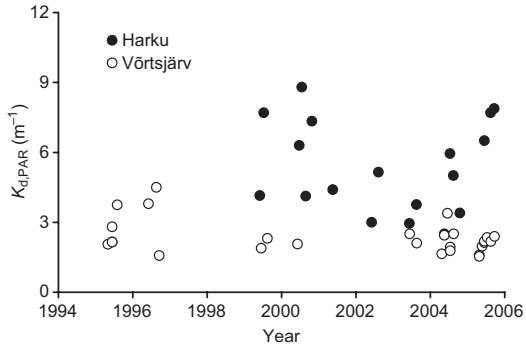

Fig. 9. Temporal variation of $K_{d,PAR}$ in Võrtsjärv and Harku, obtained from underwater measurements using the LI-192 SA.

550 nm, but it moves to the red part of the spectrum in brown-water lakes.

Additionally, the underwater light field was studied using two quantum sensors, LI-192 SA (downwelling planar irradiance, $q_{d,PAR}$) and LI-193 SA (scalar irradiance, $q_{0,PAR}$) both measuring the quantum irradiance in the PAR band of the spectrum. However, we do not have these results for all the cases shown in Table 1, because sometimes measurements could not be made due to unsuitable weather conditions such as rain or rough water surface. Thus, we have 178 $q_{d,PAR}(z)$ profiles obtained as an average from four measurement series in each case. The number of $q_{0,PAR}(z)$ profiles is smaller (often due to technical problems).

Two examples of $q_{d,PAR}(z)$ and $q_{0,PAR}(z)$ profiles are shown in Fig. 8. Measurements were carried out in Võrtsjärv in early spring (27 April 2005) and in Harku in summer (16 June 2005), in both cases at noon. The sky was partially cloudy at Võrtsjärv and almost clear at Harku. We can see that in these two cases the water properties differ noticeably: the values of $K_{d,PAR}$ for planar and scalar irradiances were 1.65 and 1.55 m^{-1} for Võrtsjärv, respectively, but for Harku they were much larger (7.34 and 7.27 m^{-1}, respectively). These two lakes were also suitable for demonstrating the long-term variations in $K_{d,PAR}$ (Fig. 9). There were 27 values (1994–2005) of $K_{d,PAR}$ for Võrtsjärv and 18 values (1999–2005) for Harku. Seasonal variability of $K_{d,PAR}$ was smaller in any individual lake than between different lakes.

The spectra of $K_d(\lambda)$ were determined from data obtained with the LI-1800 UW. All optically active components affect irradiance in a different manner; therefore the spectral K_d could give much more information on the underwater light field than the broad-band K_d. One example for each lake was chosen to show the variability among our lakes (Fig. 10a and b). The spectra for lakes comparable with Jerlov's (Jerlov 1976) coastal water types 5, 7 and 9 are presented in Fig. 10a (curves 1–4). The spectra exceeding those for type 9 by Jerlov are shown in Fig. 10b (curves 5–9). The reason for the high attenuation of light can differ among lakes (e.g. in Pääjärvi it is yellow substance (CDOM), in Võrtsjärv and in Tuusulanjärvi phytoplankton blooms). Typical attenuation spectra (especially for brownish waters) show a continuous decrease in attenuation with increasing wavelength (e.g. Fig. 10b: curve 9), but in eutrophic lakes an additional attenuation peak around 680 nm is usually seen.

Some additional studies describing the underwater light climate were: (1) comparison of euphotic layer criteria in water bodies and (2) estimation of the relation between underwater irradiance and quantum irradiance in different lakes (Reinart *et al*. 1998b, 2000).

Optical classification of lakes

In addition to Jerlov's classification of water types, several versions of the optical classification of lakes were elaborated during the SUVI

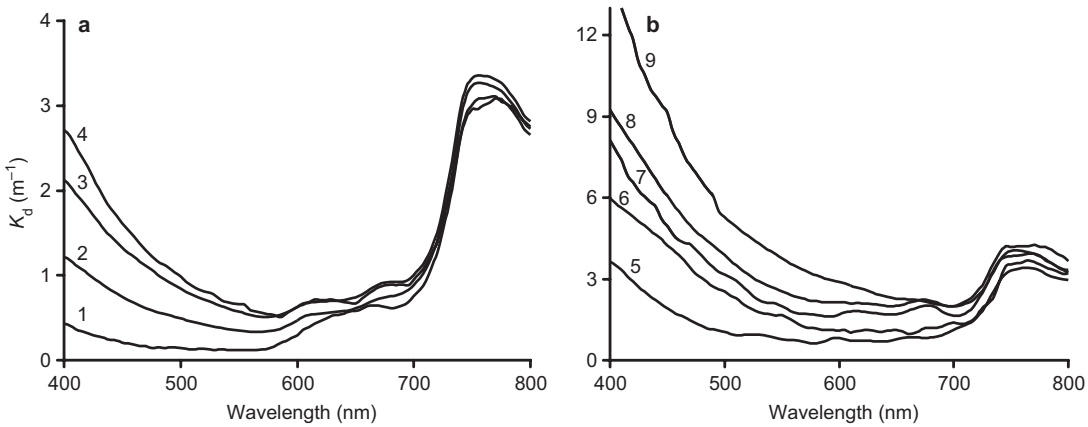

Fig. 10. Measured diffuse attenuation coefficients of light in selected lakes: (**a**) 1 = Äntu Sinijärv [K_d(490 nm) = 0.14 m^{-1}], 2 = Paukjärv (0.53 m^{-1}), 3 = Koorküla Valgjärv (0.92 m^{-1}), 4 = Vesijärvi (1.1 m^{-1}); (**b**) 5 = Päijänne (1.13 m^{-1}), 6 = Lammi Pääjärvi (2.72 m^{-1}), 7 = Vôrtsjärv (4.0 m^{-1}), 8 = Tuusulanjärvi (4.2 m^{-1}), 9 = Valkekotinen (5.6 m^{-1}). The thick part of some spectra is calculated by method Reinart and Herlevi (1999).

project (Reinart 2000, Reinart *et al*. 2003, Arst 2003). The first classification version by Reinart *et al*. (2003) is based on the apparent optical properties in the PAR region and the amount of OAS. The criterion for including a particular water body in a certain optical class was found using a K-means clustering technique (Reinart *et al*. 2003). As a result, five optical classes were determined. In lakes belonging to class C (CLEAR) the amount of OAS is smallest of all lake classes. Their waters are transparent and $K_{d,PAR}$ is the smallest. The optical properties of the water are influenced mainly by phytoplankton pigments. These waters may often be comparable with coastal ocean waters. In class M (MODERATE) lakes the water is darkened mainly due to the presence of yellow substance, which in the M class is the most important factor affecting the light field. In these lakes absorption processes are relatively more important than scattering. A total of 69% of all lakes investigated belonged to classes C and M. Class T (TURBID) includes turbid, but not very eutrophied lakes. Suspended particles (both organic and mineral) cause high scattering and backscattering. Class V (VERY TURBID) lakes are characterized by a very high C_{chl} (> 60 mg m^{-3}) and frequent appearance of phytoplankton blooms. Class V is very typical of shallow eutrophic lakes, as shown elsewhere (Kirk 1981, Dekker *et al*. 1995). Class B (BROWN) comprises humic lakes, in which the amount of dissolved organic matter is so high that the water is actually brown. In these lakes $K_{d,PAR}$ is very high (as shown by measurements in Nohipalu Mustjärv it can be more than 7 m^{-1}).

The second classification system made by Reinart *et al*. (2003) is based on the irradiance reflectance spectra just below the water surface (measurement data in Estonian and Finnish lakes). The results obtained showed that lakes are highly reflective in the green and red regions of the spectrum, but the absolute values of reflectance and its spectral shape may differ greatly. Five types (C_R, M_R, T_R, V_R and B_R) and one subtype (MB_R) were distinguished. A detailed description (numerical data on the irradiance reflectance (R_D) spectra and the location of spectral maxima) of lakes corresponding to each type is presented in Reinart *et al*. (2003).

In Arst (2003) a third version of the optical classification of lakes was elaborated, relying on light attenuation in the water and the predominant OAS as basic variables. These basic characteristics are c^*_{PAR} and the ratio $C_{chl}^{0.66}/c^*_f$(380 nm). The reason for including this ratio is to estimate (and compare) the relative influence of two important OAS (phytoplankton and CDOM) on water transparency. Thus, when this ratio is high the predominant substance is phytoplankton; when it is low CDOM predominates. The exponent 0.66 was used, taking into account that in the formulas by Baranov (1979) and Maritorena

et al. (2000) the absorption coefficient of phytoplankton was proportional to $C_{chl}^{0.667}$ and $C_{chl}^{0.65}$, respectively. Logically, for this classification, instead of $C_{chl}^{0.66}/c^*_f(380\ nm)$ the ratio $a_{chl,PAR}/a_{CDOM,PAR}$ should to be used. However, the measurement results of C_{chl} and the spectral attenuation coefficient of filtered water are quite often available, but the data on absorption coefficients of each OAS, averaged over the PAR region, are rather scarce. The values of the basic parameters of this classification are given in Table 3.

The final classification will be performed by linking two types of classes. For instance, class 'M+Y(Chl)' means that the lake is of moderate transparency, but the predominant OAS is yellow substance, the influence of chlorophyll being not as high. Class 'ELT+Chl' can be interpreted as extremely turbid water, in which chlorophyll predominates. Class 'ELT+YY' is a lake of extremely low transparency with a very high concentration of CDOM. The data for 15 Estonian and Finnish lakes used for classification, and their optical classes are presented in Arst (2003).

Models elaborated for determining the K_d spectra and underwater light field

Following the slightly modified method introduced by Austin and Petzold (1986), Reinart and Herlevi (1999) developed an analytical expression for $K_d(\lambda)$ in the range 400–800 nm, taking the value of K_d at 490 nm as a reference value. The slope parameter $M(\lambda)$ and the intercept $J(\lambda)$ for all wavelengths were based on the fitting by least squares technique of a linear equation of the form:

$$K_d(\lambda) = J(\lambda) + M(\lambda) + K_d(490) \qquad (14)$$

In Table 4 the values of the parameters $J(\lambda)$ and $M(\lambda)$ are presented in 10-nm steps in which

Table 3. Classification of lake waters by c^*_{PAR} and $C_{chl}^{0.66}/c^*_f(380\ nm)$. The respective Secchi disk depth ranges are also shown.

First classification variable				Second classification variable	
Class by c^*_{PAR} (or z_{SD})	Code	c^*_{PAR} (m^{-1})	z_{SD} (m)	Class by OAS (code)	$C_{chl}^{0.66}/c^*_f(380\ nm)$
Clear	C	0.8–1.5	7–3.5	Chl	> 2
Moderate	M	1.5–3	3.5–2	Chl(Y)	1–2
Low transparency	LT	3–7	2–1	Y(Chl)	0.5–1
Very low transparency	VLT	7–15	1–0.5	Y	0.1–0.5
Extremely low transparency	ELT	> 15	< 0.5	YY	< 0.1

Table 4. Values of intercept $J(\lambda)$ (± 0.04) and slope parameter $M(\lambda)$ (± 0.01) for analytical expression of $K_d(\lambda)$ by Eq. 13 (Reinart and Herlevi 1999).

λ (nm)	$J(\lambda)$	$M(\lambda)$	λ (nm)	$J(\lambda)$	$M(\lambda)$	λ (nm)	$J(\lambda)$	$M(\lambda)$
400	0.58	2.20	510	–0.07	0.87	610	0.03	0.51
410	0.52	2.00	520	–0.08	0.80	620	0.08	0.50
420	0.44	1.79	530	–0.09	0.74	630	0.10	0.47
430	0.37	1.66	540	–0.10	0.68	640	0.12	0.45
440	0.28	1.56	550	–0.11	0.64	650	0.16	0.43
450	0.22	1.37	560	–0.13	0.61	660	0.21	0.43
460	0.18	1.24	570	–0.14	0.58	670	0.26	0.44
470	0.11	1.14	580	–0.12	0.56	680	0.31	0.43
480	0.06	1.06	590	–0.06	0.53	690	0.40	0.38
490	0.00	1.00	600	0.00	0.52	700	0.53	0.33
500	–0.04	0.93						

the entire spectrum of $K_d(\lambda)$ could be found by the reference value of K_d at 490 nm. The wavelength 490 nm was chosen because the ocean colour satellites Sea-viewing Wide Field-of-View Sensor (SeaWiFS) and Moderate Resolution Imaging Spectroradiometer (MODIS) provide K_d(490 nm) as a standard Level 2 product (http://oceancolor.gsfc.nasa.gov/), and many widely used instruments have this waveband. Thus, using Eq. 14 and the 'satellite' value of K_d(490), we can recreate the entire spectrum in the PAR region. This is especially important for turbid and humic lakes, where in the violet and blue parts of the spectrum the values of underwater light are often very low and practically no measurement data are available. The generalized version of Eq. 14 is presented as Eq. 15 (Reinart and Herlevi 1999), in which the spectra of $K_d(\lambda)$ can be recreated taking the reference wavelength not only as 490 nm, but also as any other wavelength. Note that for each case the same coefficients as shown in Table 4 must be used.

$$K_d(\lambda_2) = J(\lambda_2) + \left[K_d(\lambda_1) - J(\lambda_1)\right]\frac{M(\lambda_2)}{M(\lambda_1)} \quad (15)$$

The main disadvantage of the analytical formula (Eq. 14) was that it did not describe well those lakes with very clear, turbid or brownish waters. One of the reasons may be that our dataset did not contain enough such examples, but the main reason is probably that one parameter, K_d(490 nm), is not enough to fully describe optically multicomponential waters. A study for estimating the validation of the 490 model was carried out by Paavel *et al*. (2006). In many individual cases, the results obtained using the 490 model were in good accordance with measured values obtained throughout the PAR region, but often some discrepancies in the blue and red regions were observed. Usually the overestimation of $K_d(\lambda)$ in the blue region is accompanied by underestimation of $K_d(\lambda)$ in the red region, or *vice versa*. The characteristics of these discrepancies lead to the conclusion that in computing the average PAR values of $K_d(\lambda)$ the measured and modelled values of the data should be similar (errors in the blue and red regions should compensate for each other). We compared the measured values of $K_{d,PAR}$ ($K_{d,PAR}$(measured)) with those obtained with the 490-model ($K_{d,PAR}$(490 model)). Indeed, the correlation $K_{d,PAR}$(measured) *vs*. $K_{d,PAR}$(490 model) gives the regression formula $y = 0.983x$ (R^2 = 0.996, SD = 0.108 m^{-1} and $p < 0.00002$).

Since the various OAS have specific spectral effects on $K_{d,\lambda}$, it may be better to use not one but several reference wavelengths. Relying on Eqs. 14 and 15, we elaborated a method combining the spectra obtained for three different wavelengths (C-model) that allowed us to recreate the spectrum of $K_{d,\lambda}$ (Paavel *et al*. 2006). We chose those wavelengths corresponding to the centres of three wavebands of the BIC-2104 radiometer (412, 555 and 665 nm). Since the parameters $J(\lambda_r)$ and $M(\lambda_r)$ were presented in 10-nm steps (Table 4), the necessary values of these parameters were determined with linear interpolation. Currently, we use the following computing system for the C-model (λ in nm, $K_{d,\lambda}$ in m^{-1}):

1. Interval 400–435 nm: take $K_{d,\lambda}$ obtained from the 412-model.
2. Interval 435–525 nm:

$$K_{d,\lambda} = [0.5 + 0.01(480 - \lambda)]K_{d,\lambda}(\lambda_r = 412) + [0.5 - 0.01(480 - \lambda)]K_{d,\lambda}(\lambda_r = 555)$$

3. Interval 525–595 nm: take $K_{d,\lambda}$ obtained from the 555-model.
4. Interval 595–655 nm:

$$K_{d,\lambda} = [0.5 + 0.01(640 - \lambda)]K_{d,\lambda}(\lambda_r = 555) + [0.5 - 0.01(640 - \lambda)]K_{d,\lambda}(\lambda_r = 665)$$

5. Interval 655–700 nm: take $K_{d,\lambda}$ obtained from the 665-model.

We calculated the statistical characteristics of the regression $K_{d,\lambda}$(measured) *vs*. $K_{d,\lambda}$(C-model) determined for 11 wavelengths in the PAR region of the spectrum. For all wavelengths $N = 84$ and significance $p < 10^{-71}$. The intercept was taken equal to zero, and the regression formula for $K_{d,\lambda}$(measured) *vs*. $K_{d,\lambda}$(C-model) was in the form $y = C_1x$. Coefficient C_1 varied from 0.997 to 1.016, R^2 from 0.977 to 0.998, and the relative error was between –0.032 and 0.021 m^{-1} (Paavel *et al*. 2006). Thus, the C-model allowed us to determine the values of $K_{d,PAR}$ with very high accuracy (the coefficient of the regression for-

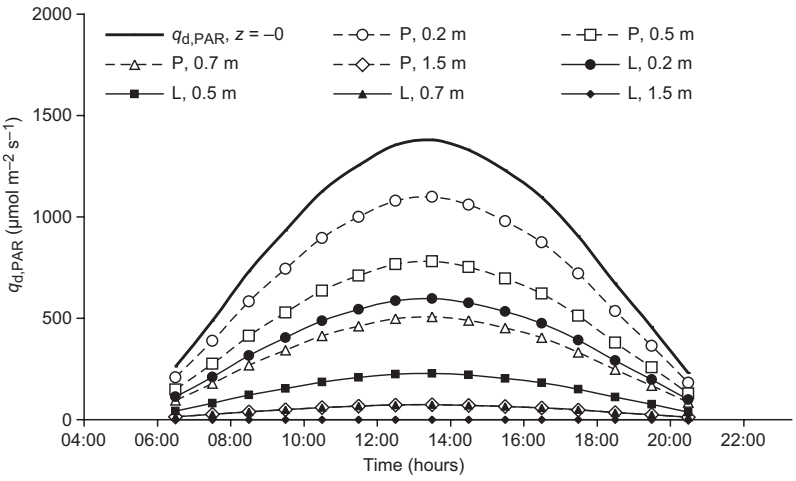

Fig. 11. Diurnal vatiation of quantum irradiance (q_{PAR}) on 15 May 1998 in Päijänne and Lohjanjärvi (station 2) at different depths, calculated by our semi-empirical model. In both cases the sky was assumed to be clear during the whole day.

mula was 1.001, R^2 = 0.9986 and SD = 0.0604 m^{-1}).

A semiempirical model for quantitative description of the spectral, temporal and spatial variations of the underwater light field was elaborated and its mathematical realization presented in Arst *et al*. (1997b, 2002) and Arst (2003). This model allowed us to calculate the values of underwater irradiance relying on the data on (1) light attenuation coefficient spectra determined in the laboratory from episodically taken water samples, and (2) incident solar irradiance recorded throughout the observation period (day, week, month, etc.). The result was the quantitative description of the underwater light regime for one or several objects. The main advantage of the respective automated computation system is the feasibility of acquiring large amounts of data describing the underwater light field, based on simple measurements. The results of this system also include the values of quantum irradiance necessary for the computation of primary production. This model is useful when measurements of the underwater irradiance *in situ* are impossible due to weather conditions. Monitoring of radiation by several underwater spectroradiometers at buoy stations is technically complicated and expensive.

Several examples of the results obtained with the model are presented in Arst (2003). These include diurnal and spectral variation in $E_d(z,\lambda)$, diurnal variation in $E_{d,PAR}(z)$ at different depths during a 2-week period in summer 2001 (Maardu), the corresponding daily sums of $E_{d,PAR}(z)$, and monthly sums of solar energy at different depths for June, July, August and September 2001 in two SUVI lakes.

In the present paper, we add a further example describing the diurnal variation in q_{PAR} on 15 May 1998 in Päijänne and Lohjanjärvi (station 2). Unfortunately, we had only water-sample data and no information on change in incident irradiation during this day. However, since the day was sunny, we used estimated values of incident quantum irradiance for clear weather, relying on its average values at 60°15´N and 24°30´E, which are rather similar to those at Lohjanjärvi and the southern part of Päijänne. We obtained these average values from 'Oceanographic Tables' (1975) for moderate transparency of the atmosphere. The results (Fig. 11) show that the attenuation of solar light in Lohjanjärvi exceeds markedly that in Päijänne: in the latter case q_{PAR} at a depth of 0.2 m is almost two times higher than that in Lohjanjärvi, while at a depth of 1.5 m q_{PAR} in Päijänne is practically equal to that at 0.7 m in Lohjanjärvi. Note that the Secchi depth values for Päijänne and Lohjanjärvi (station 2) were respectively 6.5 m and 0.7 m.

Optical remote sensing of lakes

Some examples of our remote-sensing measurement results are presented in Fig. 12. Since information that gives the shape of the spectral

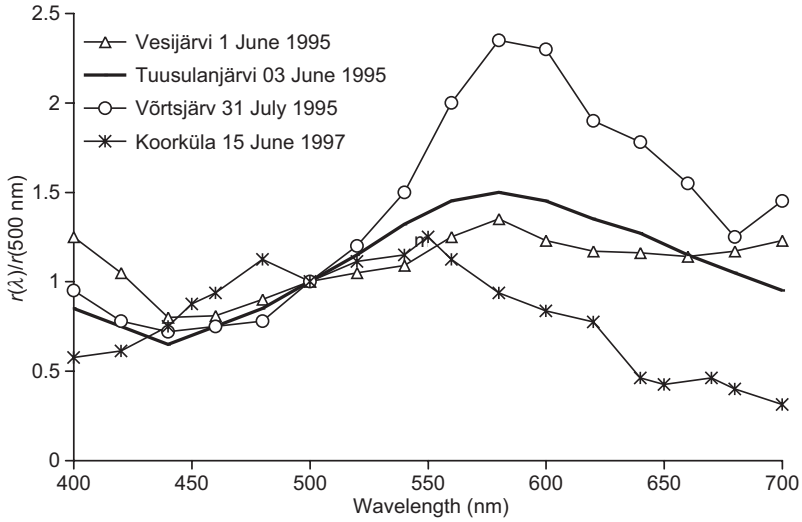

Fig. 12. Spectral distribution of remote sensing reflectance, $r(\lambda)$, normalized to 500 nm for Vesijärvi, Tuusulanjärvi, Võrtsjärv and Koorküla Valgjärv.

curve in remote sensing is especially important, the values of $r(\lambda)$ normalized to 500 nm are shown. Note that the four lakes presented here are characterized by the following values of the Secchi depth z_{SD}: Vesijärvi, z_{SD} = 2.5 m, Tuusulanjärvi, z_{SD} = 0.9 m, Võrtsjärv, z_{SD} = 0.8 m and Koorküla Valgjärv, z_{SD} = 4.5 m. The spectra differ from each other markedly: in clear-water Koorküla Valgjärv the values for $r(\lambda)/r$(500 nm) are smallest in the 560–700-nm band, for Võrtsjärv (during the algal bloom in August) the values in this band for $r(\lambda)/r$(500 nm) are much higher than for any other lake. In Võrtsjärv the minimum in the spectrum caused by the chlorophyll absorption band near 675 nm is clearly seen. Our remote-sensing measurement results were published elsewhere (Kutser 1997, 2004, Kutser *et al*. 1996, 1997a, 1997b, 1998, 1999, 2006, Arst *et al*. 1999c, Leppäranta *et al*. 1999, Erm *et al*. 2001, Reinart and Kutser 2006).

The remote-sensing data were used to develop empirical algorithms (band ratios, their combinations and more sophisticated colour algorithms) for estimating chlorophyll, CDOM and suspended matter concentrations, as well as Secchi disk depth and the beam attenuation coefficient from remotely measured data. Some of the proposed algorithms are presented in Kutser (1997) and Kutser *et al*. (1998).

Analysis showed seasonal variability in performance of the band-ratio type algorithms and relatively wide variability among expeditions. Therefore we initiated development of a bio-optical model for interpretation of remote-sensing data. The model allows simulation of the reflectance spectra based on the concentrations of chlorophyll, CDOM and suspended matter. We assumed that if a modelled spectrum is similar to a remote-sensing spectrum then the concentrations of OAS used to simulate the most similar spectrum match with those found in the water body. Model development began with the parameters and data available in the literature. We gradually tuned the model with the SUVI data. We were also able to estimate several parameters that were not measurable *in situ* at the time (backscattering coefficient spectra) or hardly known (scattering coefficient spectra), thus filling in the unknowns in the model with actual measurement data (Kutser 1997). The results obtained with the model were published in Kutser (1997) and Kutser *et al*. (1996, 1998, 2001).

The most recent version of the model is described in Kutser *et al*. (2001) and was based on the following equations (Gordon *et al*. 1975, Kirk 1984):

$$R_D(0^-,\lambda) = C(\mu_0)\frac{b_b(\lambda)}{a(\lambda)+b_b(\lambda)} \qquad (16)$$

where $R_D(0^-,\lambda)$ is the irradiance reflectance just beneath the water surface, b_b is the backscatter-

ing coefficient, μ_0 is the cosine of the solar zenith angle and

$$C(\mu_0) = -0.629\mu_0 + 0.975 \quad (17)$$

As light passes through the water–air interface it undergoes refraction that increases its angle to the vertical. Combining these effects with the effect of internal reflection, Austin (1980) proposed a factor of 0.544 for relating radiance just above the surface with radiance just below the surface. Thus, we can calculate the diffuse component of remote-sensing reflectance just above the water surface:

$$r_D(\lambda) = 0.544(-0.629\mu_0 + 0.975)\frac{b_b(\lambda)}{a(\lambda)+b_b(\lambda)}. \quad (18)$$

The total absorption (a) and backscattering (b_b) coefficients are additive over the constituents of the medium by the definition of inherent optical properties (which requires the absence of multiple interactions). We assumed that there are three optically active components in the water: phytoplankton, CDOM and suspended matter. Thus the values of a and b_b were determined as the sums of the respective parameters of these substances.

Models similar to that described above were proposed by a number of authors (*see* list of models in Dekker *et al*. [2001]). The main differences between the models are in the number of OAS and the specific absorption and backscattering coefficients used. The amount of CDOM, as well as absorption and backscattering due to suspended matter are often expressed through the empirical functions of C_{Chl}. This is acceptable in oceanic waters, but not in coastal and inland waters where the concentrations of other OAS are not correlated with C_{Chl}.

Currently, optical remote sensing results are mostly obtained by satellites, which allow large areas to be described, and the individual spectra for some sampling stations are used only as ground-truth data for calibration of measurements from space. However, the technical limitations related to spatial, spectral and radiometric resolution of the instruments are mainly responsible for the serious difficulties so far encountered in describing the lakes (even large ones) using satellite images.

Studies in ice-covered lakes: ice structure and radiative characteristics

Structure of lake ice cover

In Finnish and Estonian Lakes the ice cover is static, apart from very early and late in the ice season. An exception to this rule is Lake Peipsi, where mechanical, wind-driven shifts are observed. A static ice cover consists of three principal layers: snow, snow-ice and congelation ice. The total thickness of ice is 10–100 cm, and the thickness of snow on top of the ice is 0–50 cm. Snow-ice is formed by freezing of wetted snow; it inherits air bubbles from the snow layer and therefore appears whitish and is also sometimes called white ice. Congelation ice is formed of lake water only. Sometimes a slush layer is found on top of the snow-ice or between the snow-ice and congelation ice. Solar radiation is a very important source of heat for the ice, snow and water beneath the ice and triggers the start-up of the spring melting period (e.g., Leppäranta 1995).

The structure and physical properties of ice and snow and concentrations of sediments and other impurities in the ice of the Baltic Sea and some Finnish lakes have been examined since the 1960s (Palosuo 1965, Leppäranta *et al*. 1998b, Leppäranta and Kosloff 2000). The ice season was included in the SUVI lake field programme in year 2000 (Leppäranta *et al*. 2001, Erm *et al*. 2002, Leppäranta *et al*. 2003a). Activities in Santala Bay in the Gulf of Finland were initiated 2 years earlier and provided a good sea ice (or brackish ice) reference (Kawamura *et al*. 2001, 2002, Rasmus *et al*. 2002, Granskog *et al*. 2004). As is known, the principal difference between sea ice and lake ice is that the former contains brine channels, where phytoplankton may grow.

The structure of ice in the study sites showed basically the two-layer structure with snow-ice and congelation ice. Sea ice samples contained brine channels, which do not exist in lake ice (Fig. 13a). Lake ice was more homogeneous in Paukjärv (Fig. 13d), but sometimes there were many distinctive layers (Fig. 13b and c). In addition, optically thicker layers may appear both at the top and inside the sheet of lake ice. The

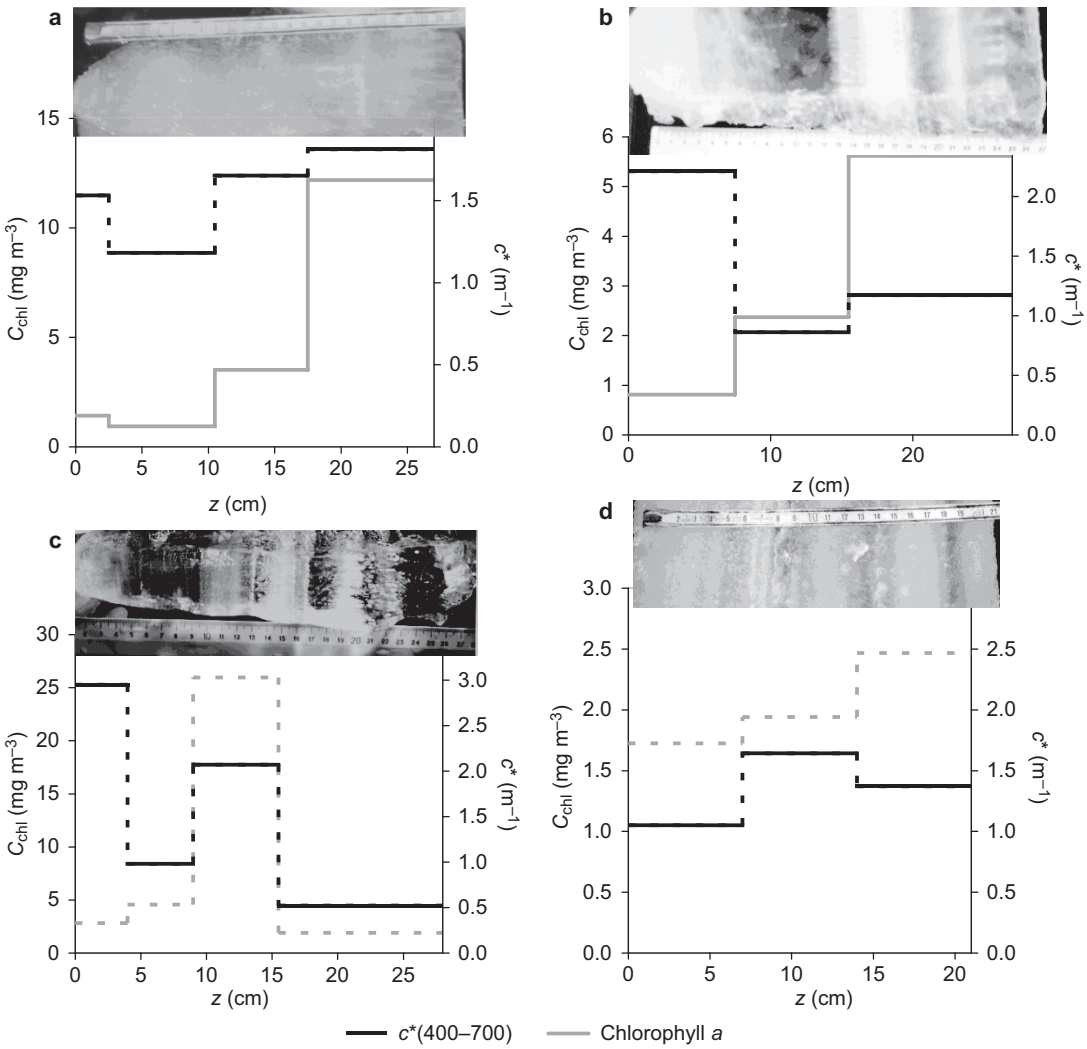

Fig. 13. Vertical cross-section of ice sheet in normal light and the profiles of chlorophyll *a* and beam attenuation coefficient c^*_{PAR} of melt water: (**a**) Santala Bay (16 March 2000), (**b**) Lake Ülemiste (15 February 2000), (**c**) Lake Maardu (8 March 2000), (**d**) Paukjärv (23 February 2000); $z = 0$ refers to the top surface.

reasons for appearance of such a structure could be different formation conditions (fast or slow freezing, snow ice), precipitation consisting of impurities (acid, ash, etc.), and melting–freezing cycles. The figure also shows chlorophyll *a* and the beam attenuation coefficient determined from the melt water of ice slices, and these are highly correlated.

Impurities in the lake ice cover were mapped in 1996–1998 in four Finnish lakes together with those in the water beneath the ice (Table 5). The main routes for accumulation impurities are atmospheric fallout and flooding of the ice sheet by lake water (Leppäranta *et al*. 1998b, Leppäranta *et al*. 2003b). The situation is similar in the landfast ice zone on the coast of the Gulf of Finland (Leppäranta *et al*. 1998a). Congelation ice growth at the bottom of the ice rejects the impurities efficiently. In general the level of dissolved matter in the lake ice meltwater was 15%–30% of that in the lake water itself and close to the level in snow. For suspended matter lake water and ice showed similar levels, but in two cases suspended matter in snow had much

larger level. Considering the role of optically active substances, lake ice has less yellow substance than lake water, and in the absence of gas bubbles the ice may be more transparent than the lake water. In the brackish Santala Bay, the ice is more porous and there is chlorophyll in the brine pockets. Consequently, the transparency is much lower than in lake ice.

However, care should be taken when interpretating the properties of the meltwater. Major changes in the water samples during melting–freezing cycles (as illustrated in Fig. 14) was observed in the previous work by Erm *at al*. (2003). One problem in the analysis of meltwater samples may be the precipitation of salts from the water by freezing process — the energy barrier of such processes may by very high and accordingly the time constant millions of years, especially for the CaMg carbonates.

Radiative characteristics of the ice cover

Albedo (A) is, by definition, the ratio of upwelling total (integrated over the wavelength) irradiance to downwelling total irradiance at the surface. Our results describing the influence of surface conditions on the albedo of ice-covered lakes are given in Table 6. The albedo of ice varied widely (0.20–0.58), depending on the optical and physical properties of the ice and the weather conditions (grey ice, dark ice, whitish ice, melting ice, hoarfrost on the ice), it was highest for the hoarfrost case. The albedo of snow was even higher: for fresh snow it was 0.85–0.94 decreasing with aging of the snow down to about 0.63. There is considerable variation between A_{snow} and $A_{(snow\ removed)}$, mainly caused by variations in the optical properties of ice and snow. In most cases $A_{(snow\ removed)}$ exceeded 0.5, which is systematically higher than A_{ice}. This is explained not only by the greyness of some types of ice and melting ice (smaller scattering coefficients), but also by the fact that we cannot totally remove all the snow, especially in scabrous ice; some snow invariably remains on the ice and increases its albedo. Our limited database (especially for the vertical and crystalline structure of ice) did not allow us to carry out a reliable investigation into the relationships between albedo and ice microstructure. Some estimations of the spatial variation of ice albedo in the Baltic Sea (in situ and satellite data) are presented in Arst and Sipelgas (2004), time series of PAR irradiance in ice was mapped by Shirasawa *et al*. (2001), and a specific case study on the albedo of thin ice was performed by Ishikawa *et al*. (2003).

Snow was the main factor involved in the reduction of irradiance during its penetration through the snow/ice cover (Table 6). The transmissivity increased 2.5–20 times after removing the snow. The diffuse attenuation coefficient in PAR band for lake ice ($K_{d,i}$) was in some cases higher and in some cases lower than that for liquid water ($K_{d,w}$); the ratio $K_{d,i}/K_{d,w}$ was 0.3–1.8.

The value of $K_{d,w}$ increased after removing the snow from the ice cover. One reason may be that the spectral composition of irradiance below the snow and ice layer is different from that below the ice cover or that changes may have occurred in the angular distribution of light after removing the snow. The euphotic zone (the water layer where photosynthesis occurs) is usu-

Table 5. Mean conductivity, dissolved matter and suspended matter in lake ice meltwater (I), meltwater of snow on ice (S), and lake water surface layer (W). The data were collected in four lakes in March, years 1996–1998. (Leppäranta *et al.* 2003b).

	Conductivity μS cm^{-1} [25 °C]			Dissolved matter (mg l^{-1})			Suspended matter (mg l^{-1})		
	I	S	W	I	S	W	I	S	W
Pääjärvi	13	17	108	14	15	64	2.1	4.2	3.7
Päijänne	8	19	79	11	20	31	2.1	7.0	1.4
Vesijärvi	7	28	128	13	24	52	2.0	9.9	1.1
Tuusulanjärvi	15	10	208	17	17	143	12.6	11.6	11.5

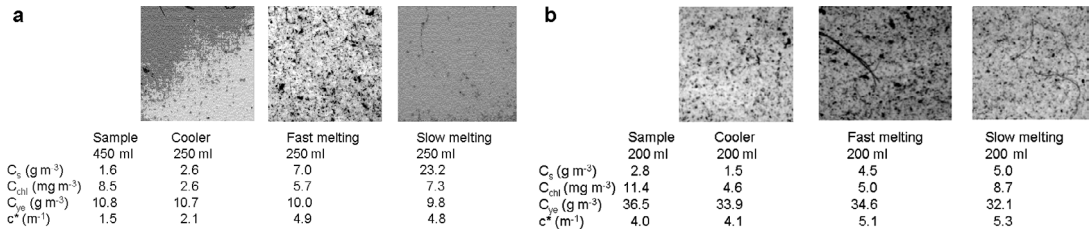

	Sample 450 ml	Cooler 250 ml	Fast melting 250 ml	Slow melting 250 ml
C_s (g m^{-3})	1.6	2.6	7.0	23.2
C_{chl} (mg m^{-3})	8.5	2.6	5.7	7.3
C_{ye} (g m^{-3})	10.8	10.7	10.0	9.8
c^* (m^{-1})	1.5	2.1	4.9	4.8

	Sample 200 ml	Cooler 200 ml	Fast melting 200 ml	Slow melting 200 ml
C_s (g m^{-3})	2.8	1.5	4.5	5.0
C_{chl} (mg m^{-3})	11.4	4.6	5.0	8.7
C_{ye} (g m^{-3})	36.5	33.9	34.6	32.1
c^* (m^{-1})	4.0	4.1	5.1	5.3

Fig. 14. Microphotographs (natural image width 3 mm) of filtered suspended matter and corresponding concentrations of optically active substances and values of c^*_{PAR} in (**a**) Lake Ülemiste (30 Jan. 2001), and (**b**) Lake Harku (29 Jan. 2001).

ally treated as the layer at whose lower boundary PAR falls to 1% of that just below the water surface. In ice conditions, the attenuation of light in ice and snow needs to be considered and therefore the euphotic depth is much less than in open water conditions. Here this depth varied from 0.53 to 4.7 m in snow-free cases and from zero to 1.3 m in snow-covered cases.

A suitable parameter for the angular structure of under-ice light field is the ratio of planar to scalar quantum irradiances $q_{d,PAR}/q_{0,PAR}$ (Arst *et al*. 2006). This ratio is dependent on the incident solar irradiance, solar zenith angle, and absorption and scattering in the ice, snow and water. In the upper layers of an ice-free water body the ratio $q_{d,PAR}/q_{0,PAR}$ generally decreases with increasing depth, with numerical values usually between 0.4 and 0.9 (Reinart 2000). The situation can be different in under-ice waters, because the light having just penetrated the ice layer is considerably more diffuse than that below the surface of the ice-free water. In contrast to ice-free situations, scalar irradiance decreases with increasing depth more rapidly than planar irradiance. This means that the diffuse attenuation coefficient for scalar irradiance in under-ice water exceeds that for planar irradiance.

Thus the influence of snow/ice cover causes radiation to be highly diffuse just under the ice. Under ice-free conditions (on clear days) the asymptotic state of the angular structure of light is usually attained at deeper layers, but in ice-covered waters the profiles of $q_{d,PAR}/q_{0,PAR}$ are already 'asymptotic' beginning at the lower sur-

Table 6. Values of the albedo (A), vertically averaged attenuation coefficient of light for ice ($K_{d,i}$) and diffuse attenuation coefficient for under-ice water ($K_{d,w}$), all for the PAR region of the spectrum. Only those cases without snow are presented, D_i is the thickness of the ice layer.

Lake	Time	D_i (cm)	A	$K_{d,i}$ (m^{-1})	$K_{d,w}$ (m^{-1})	Comments
Ülemiste	04 Feb. 2000	24	–	–	2.12	Snow removed
	15 Feb. 2000	27	–	–	1.77	Snow removed
	23 Mar. 2000	28	–	–	1.71	Snow removed
	30 Jan. 2001	23	0.30	0.50	1.31	Snow removed
	12 Feb. 2001	27	0.20	1.04	0.79	Dark grey, smooth ice
	30 Jan. 2002	42	0.70	1.80	1.32	Scabrous ice, snow removed
Maardu	08 Mar. 2000	28	–	–	0.88	Hoarfrost on the ice
	31 Jan. 2001	24	0.37	0.56	0.95	Snow removed, wet grey ice
	20 Feb. 2001	28.5	0.22	1.46	0.80	Remains of slush on ice
	30 Jan. 2002	41.5	0.48	0.56	1.12	Snow removed
	24 Feb. 2002	33	0.58	1.83	0.99	Snow removed
Harku	03 Feb. 2000	22	–	–	2.12	Snow removed
	19 Feb. 2001	22	0.26	1.43	1.60	Dark grey, smooth ice
	22 Feb. 2002	27	0.26	1.41	1.87	Dark grey, smooth ice
Pääjärvi	18 Mar. 2003	76	0.29	0.46	1.42	Dark grey, smooth ice
Valkeakotinen	19 Mar. 2003	57	0.43	3.54	2.23	Snow removed, yellowish ice
Ormajärvi	20 Mar. 2003	74	0.58	0.82	0.56	Hoarfrost on ice

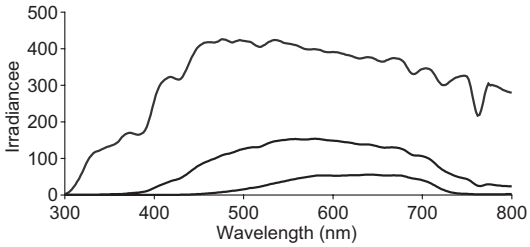

Fig. 15. Downwelling irradiance spectra (mW m^{-2} nm^{-1}) at the ice surface (albedo of 0.5 applied) (top line), 15 cm beneath the ice (middle line), and 1 m beneath the ice (low line) in Pääjärvi on 14 April 2004. The ice was bare, thickness 33 cm.

face of the ice. It is also important to realize that in ice-free water the radiation falling on the surface of the 'asymptotic layer' originates from the same medium (water), but the radiation below the ice comes from a different medium (ice). The scattering properties of ice are much different in comparison to those of the water.

A dry snow layer has a weak influence on the spectral characteristics of light, since in the optical band reflection and scattering are practically independent of the wavelength. Gas pockets are the principal scatterers and they are much larger than the wavelength of light. Wet snow includes liquid water with its properties of strongly absorbing long optical waves and consequently the light spectrum becomes modified. The influence of ice on spectral composition is between those of snow and clear water, depending on the volume of the gas pockets. Figure 15 illustrates the spectral attenuation of the ice based on measurements above and beneath the ice in Pääjärvi springtime. The level is even across the band 500–700 nm and drops down in the lower and higher ends of the light spectrum. When going deeper into the water, the humic Pääjärvi water absorbs short waves out from the light. Consequently, from the point of view of light conditions in the water, the ice cover lowers the light level and makes a more diffuse directional distribution, and modifies the spectra by relative lowering of for short and long waves.

We can ask whether the beam attenuation coefficient (c_{ice}) as well as the diffuse attenuation coefficient ($K_{d,ice}$) for an ice layer can be estimated using the data obtained from meltwater. As is generally known, the beam attenuation coefficient of ice and meltwater (c_{melt}) can be expressed as the sum of the respective absorption and scattering coefficients, a and b:

$$c_{ice} = a_{ice} + b_{ice} \quad (19)$$

$$c_{melt} = a_{melt} + b_{melt} \quad (20)$$

We can probably hypothesize that there may be some correlation between a_{ice} and a_{melt}, but we cannot do it for b_{ice} and b_{melt}. In meltwater b is mainly determined by the scattering properties and amount of suspended matter. In an ice layer b_{ice} is strongly influenced by the crystalline structure of ice: due to multiple scattering of light by ice crystals and gas bubbles the value of b_{ice} is very different from the corresponding b_{melt}. Consequently, we can estimate neither c_{ice} nor $K_{d,ice}$ from the corresponding meltwater data. This conclusion is also supported by our long-term measurement data, which showed that the correlations between the optical properties of ice and the corresponding meltwater were low.

Conclusions

1. Profound analysis of a dataset containing the concentrations of three main OAS, c^*_{PAR}, $K_{d,PAR}$ and z_{SD} in 14 Estonian and seven Finnish lakes between 1992 and 2002 was performed. The dataset obtained shows that these parameters vary among lakes and also with seasons.
2. To study the possible long-term changes in the bio-optical parameters in lakes, we had only five lakes in which the observation period is seven years or more. In two Finnish lakes (Pääjärvi and Vesijärvi) the chlorophyll content appears to increase with time, while in N. Valgjärv and Võrtsjärv seasonal variations of C_{chl} predominate. In Pääjärvi, Vesijärvi, N. Valgjärv and Võrtsjärv the concentration of CDOM and the Secchi depth showed practically no long-term trend in all four lakes.
3. The multiple regression c^*_{PAR} *vs.* (C_s, C_{chl}, c^*_f(380 nm)) gave the following statistical parameters: $R^2 = 0.962$, SD = 2.15 m^{-1}, and $p < 0.000001$. The regression of $K_{d,PAR}$ *vs.* z_{SD} can be described by a power function with R^2

= 0.724 and $K_{d,PAR}$ *vs.* c^*_{PAR} with linear function with $R^2 = 0.653$.

4. With the aid of measurements by the ac-9 instrument, we parametrized the spectral curve of scattering coefficient, using a power function with exponent p_b. The multiple regression p_b *vs.* (C_s, C_{chl}, c^*_f(380 nm)) gave the following statistical parameters: R^2 = 0.668, SD = 0.259 and $p < 0.000001$.
5. During 1995–2005 we also measured the spectra of downwelling and upwelling irradiance in SUVI lakes (in all 132 measurement cycles, the LI-1800 UW instrument was used). The most striking feature in many Estonian and Finnish lakes is the very rapid attenuation of irradiance with depth in the region of 400–500 nm, due to strong absorption by CDOM. Irradiance also diminishes rapidly at the red end of the spectrum (due to absorption by water itself), although not to the same extent as at the blue end. The wavelength of maximal penetrating radiation (λ_{max}) is around 550 nm, but it shifts to the red part of the spectrum in brown-water lakes.
6. We studied the underwater light field, using two quantum sensors, the LI-192 SA (planar irradiance, $q_{d,PAR}$) and LI-193 SA (scalar irradiance, $q_{0,PAR}$) both measuring the quantum irradiance in the PAR band of the spectrum. We determined the spectra of $K_d(\lambda)$ from data obtained with the LI-1800 UW and found the vertical profiles of $K_{d,PAR}$ based on the LI-192 SA data. Since all optically active components affect irradiance in a different manner, the spectral values of K_d could give much more information on the underwater light field than the broad-band $K_{d,PAR}$.
7. We elaborated three versions of the optical classification of lake waters, based on: (a) the apparent optical properties in the PAR region and the amount of OAS, (b) the irradiance reflectance spectra just below the water surface, (c) light attenuation coefficient in the water and the predominant OAS.
8. We developed two models for determining the $K_d(\lambda)$ spectra: (a) based on $K_d(\lambda)$ values for one wavelength in the PAR region; (b) based on $K_d(\lambda)$ values for three wavelengths in the PAR region (an improved version).
9. We elaborated a semi-empirical model for quantitative description of the underwater light regime. This model allowed us to calculate the values of underwater irradiance using data on (a) light attenuation coefficient spectra determined in the laboratory from episodically taken water samples, and (b) incident solar irradiance recorded throughout the observation period (day, week, month, etc.).
10. We used the remote sensing data to develop empirical algorithms (band ratios, their combinations and more sophisticated colour algorithms) for estimating OAS as well as Secchi depth and the beam attenuation coefficient from remote-sensing reflectance. We developed a bio-optical model for interpretation of remote sensing data that allowed simulation of the reflectance spectra based on the concentrations of OAS. We assumed that if a modelled spectrum is similar to a remote-sensing spectrum, the concentrations of OAS used to simulate the most similar spectrum will match with those found in the water body.
11. The wintertime experiments have shown that the under ice radiation is very strongly dependent on the snow cover on the ice due to the higher albedo and attenuation coefficient of the snow. In contrast to ice-free situations, scalar irradiance decreases with increasing depth more rapidly than planar irradiance.
12. The attenuation coefficient of ice is close to the attenuation coefficient of the lake water, and may be either larger or smaller. The correlation between optical parameters of ice and ice meltwater is quite low probably following from the scattering of gas bubbles in the ice sheet. Precipitation processes during the freezing-melting cycle may also have a notable influence on the results.

Acknowledgments: The authors are indebted to Medhat Hussainov, Sirje Mäekivi, Birgot Paavel, Liis Sipelgas, Alberto Blanco-Sequeiros, Elina Brotherus, Jens Ehn, Aija-Riitta Elo, Olli Huttunen, Antti Lindfors, Kari Pulkkinen, Kai Rasmus and Jari Uusikivi for help in the fieldwork, laboratory analyses and data processing. Dr. James Thompson is deeply thanked for a very careful language check. Financial support was provided by the Academy of Finland, Estonian Academy of Sciences, Estonian Scientific Foundation, and

the Kalle, Vilho and Yrjö Väisälä Foundation of the Finnish Academy of Sciences and Letters.

References

Arst H. 2003. *Optical properties and remote sensing of multicomponental water bodies*. Springer-Praxis Publishing, Chichester, U.K.

Arst H. & Sipelgas L. 2004. *In situ* and satellite investigations of optical properties of the ice cover in the Baltic Sea region. *Proc. Estonian Acad. Sci., Biol. Ecol.* 53: 25–36.

Arst H., Mäekivi S., Kutser T., Reinart A., Blanco-Sequeiros A., Virta J. & Nõges P. 1996. Investigation of different types of lakes in Estonia and Finland by optical methods. *Lakes and Reservoirs: Research and Management* 2: 187–198.

Arst H., Käärmann L., Arst G., Veismann U. & Kutser T. 1997a. Measuring system for passive optical remote sensing of the water bodies. *Proc. Estonian Acad. Sc., Biology and Ecology* 46: 150–163.

Arst H., Herlevi A., Lukk T. & Mäekivi S. 1997b. Calculating irradiance penetration into water bodies from the measured beam attenuation coefficient. *Limnol. Oceanogr.* 42: 379–385.

Arst H., Mäekivi S., Reinart A., Kutser T., Kallaste K., Blanco-Sequeiros A., Nõges P. & Nõges T. 1998. Water properties in some regions of the Baltic Sea and different type of lakes in Estonia and Finland. *Report Series in Geophysics* 38: 7–23.

Arst H., Erm A., Hussainov M., Kutser T., Mäekivi S., Reinart A. & Herlevi A. 1999a. Investigation of Estonian and Finnish lakes by optical measurements in 1992–97. *Proc. Estonian Acad. Sci. Biol. Ecol.* 48: 5–24.

Arst H., Erm A., Kallaste K. & Mäekivi S. 1999b. Influence of the conditions of preserving water samples and their delayed processing on the light attenuation coefficient spectra and the concentrations of water constituents. *Proc. Estonian Acad. Sci. Biol. Ecol.* 48: 149–159.

Arst H., Erm A., Kutser T. & Reinart A. 1999c. Optical remote sensing and contact measurements in Estonian and Finnish lakes in 1992–98. In: Lilover M.J. & Reinart A. (eds.), *Proc. 4th Workshop on Physical Processes in Natural Waters*, *13–17 September 1999, Roosta, Estonia*, Estonian Marine Institute, Tallinn, pp. 105–110.

Arst H., Reinart A., Erm A. & Hussainov M. 2000. Influence of the depth-dependence of PAR region diffuse attenuation coefficient on the computation results of the downward irradiance in different type of water bodies. *Geophysica* 36: 129–139.

Arst H., Erm A., Reinart A., Sipelgas L. & Herlevi A. 2002. Calculating irradiance penetration into water bodies from the measured beam attenuation coefficient II: Application of improved model to different types of lakes. *Nordic Hydrology* 33: 207–226.

Arst H., Erm A., Leppäranta M. & Reinart A. 2006. Radiative characteristics of ice-covered fresh- and brackish-water bodies. *Proc. Estonian Acad. Sci., Geology* 55: 3–23.

Austin R.W. 1980. Gulf of Mexico, ocean colour surface-truth measurements. *Boundary-layer Meteorology* 18: 269–285.

Austin R.W. & Petzold T.J. 1986. Spectral dependence of the diffuse attenuation coefficient of light in ocean waters. *Optical Engineering* 25: 471–479.

Baranov S.A. 1979. Relationship between water transparency, biomass and production of algae photosynthesis. *Journal of Hydrobiology*: 18–25.

Bricaud A., Morel A. & Prieur L. 1981. Absorption by dissolved organic matter of the sea (yellow substance) in the UV and visible domains. *Limnol. Oceanogr.* 26: 43–53.

Bricaud A., Babin M., Morel A. & Claustre H. 1995. Variability in the chlorophyll-specific absorption coefficients of natural phytoplankton: analysis and parametrization. *J. Geophys. Res.* 100(C7): 13321–13332.

Bricaud A., Roesler C. & Zaneveld J.R.V. 1995b In situ methods for measuring the inherent optical properties of ocean waters. *Limnol. Oceanogr.* 40: 393–410.

Davies-Colley R.J. & Vant W.N. 1987. Absorption of light by yellow substance in freshwater lakes. *Limnol. Oceanogr.* 32: 416–425.

Dekker A.G., Zamurovic-Nenad Z., Hoogenboom H.J. & Peters S.W.M. 1995. Remote sensing, ecological water quality modelling and in situ measurements: a case study in shallow lakes. *Hydrol. Sci.* 41: 531–547.

Dekker A.G., Brando V.E., Anstee J.M., Pinnel N., Kutser T., Hoogenboom E.J., Peters S., Pasterkamp R., Vos R., Olbert C. & Malthus T.J.M. 2001. Imaging spectrometry of water. In: van der Meer F.D. & de Jong S.M. (eds.), *Imaging spectrometry: basic principles and prospective applications*, Kluwer Academic Publishers, Dordrecht, pp. 307–359.

Dera J. 1992. *Marine physics*. PWN (Polish Scientific Publishers), Warszawa and Elsevier, Amsterdam-Oxford-New York-Tokyo.

Erm A., Arst H., Hussainov M., Kutser T. & Reinart A. 1999. Optical measurements in Lake Ülemiste. *Proc. Estonian Acad. Sci. Biol. Ecol.* 48: 63–74.

Erm A., Arst H., Trei T., Reinart A. & Hussainov M. 2001. Optical and biological properties of Lake Ülemiste, a water reservoir of the city of Tallinn I: Water transparency and optically active substances in the water. *Lakes and Reservoirs: Research and Management* 6: 63–74.

Erm A., Arst H., Nõges P., Nõges T., Reinart A. & Sipelgas L. 2002. Temporal variations in bio-optical properties of four North Estonian lakes in 1999–2000. *Geophysica* 38: 89–111.

Erm A., Reinart A., Arst H., Sipelgas L. & Leppäranta M. 2003. Optical properties of lake and sea ice. *Report Series in Geophysics* 46: 93–100.

Gallegos C.L., Jordan T.E., Hines A.H. & Weller D.E. 2005. Temporal variability of optical properties in shallow eutrophic estuary: seasonal and interannual variability. *Estuarine, Coastal and Shelf Science* 64: 156–170.

Gordon H.R., Brown O.B. & Jacobs M.M. 1975. Computed relationships between the inherent and apparent optical properties of a flat, homogenous ocean. *Appl. Optics* 14: 417–427.

Granskog M., Leppäranta M., Ehn J., Kawamura T. & Shirasawa K. 2004. Sea ice structure and properties in Santala Bay, Baltic Sea. *J. Geophys. Res.* 109, C02020.

Herlevi A. 2002a. *Inherent and apparent optical properties in relation to water quality in Nordic waters*. Ph.D. thesis, Division of Geophysics, University of Helsinki.

Herlevi A. 2002b. A study of scattering, backscattering and a hyperspectral reflectance model for boreal waters. *Geophysica* 38: 113–132.

Herlevi A., Virta J., Arst H. & Erm A. 1999. Results of light absorption measurements in Finnish and Estonian lakes in summer 1997. *Proc. Estonian Acad. Sci., Biol. Ecol.* 48: 46–62.

Ishikawa N., Takizawa A., Kawamura T., Shirasawa K. & Lepparanta M. 2003. Changes in radiation properties and heat balance with sea ice growth in Saroma lagoon and the Gulf of Finland. In: Squire V. & Langhorne P. (eds.), *Proc. 16th IAHR Ice Symp.* vol. 3, University of Otago, Dunedin, New Zealand, pp. 194–200.

Jerlov N.G. 1976. *Marine optics*. Elsevier Oceanography Series 5, Elsevier, Amsterdam-Oxford-NewYork.

Kawamura T., Shirasawa K., Ishikawa N., Lindfors A., Rasmus K., Ehn J., Leppäranta M., Martma T. & Vaikmäe R. 2001. A time series of the sea ice structure in the Baltic Sea. *Ann. Glaciol.* 33: 1–4.

Kawamura T., Granskog M.A., Lindfors A., Ehn J., Martma T., Vaikmäe R., Ishikawa N., Shirasawa K. & Leppäranta M. 2002. Study on brackish ice in the Gulf of Finland — effect of salt on sea ice structure. In: Squire V. & Langhorne P. (eds.), *Proc. 16th IAHR Ice Symp.* vol. 2, University of Otago, Dunedin, New Zealand, pp. 165–171.

Kirk J.T.O. 1984. Dependence of relationships between inherent and apparent optical properties of water on solar altitude. *Limnol. Oceanogr.* 29: 350–356.

Kirk J.T.O. 1996. *Light and photosynthesis in aquatic ecosystems*. Cambridge University Press, Cambridge.

Kutser T. 1997. Estimation of water quality in turbid inland and coastal waters by passive optical remote sensing. *Dissertationes Geophysicales Universitas Tartuensis* 8: 1–161.

Kutser T. 2004. Quantitative detection of chlorophyll in cyanobacterial blooms by satellite remote sensing. *Limnol. Oceanogr.* 49: 2179–2189.

Kutser T., Blanco A. & Arst H. 1996. Evaluation of remote sensing algorithms for the retrieval of optically-active components in turbid natural waters. *Proc. IGARSS'96,* CD-ROM.

Kutser T., Arst H., Mäekivi S., Leppänen J.-M. & Blanco-Sequeiros A. 1997a. Monitoring of algae blooms by optical remote sensing. In: Spiteri A. (ed.), *Remote sensing'96*, Balkema, Rotterdam, pp. 161–166.

Kutser T., Arst H., Mäekivi S. & Blanco-Sequeiros A. 1997b. Optical inverse problem in turbid waters. *SPIE Proceedings* 2963: 477–482.

Kutser T., Arst H., Mäekivi S. & Kallaste K. 1998. Estimation of the water quality of the Baltic Sea and some lakes in Estonia and Finland by passive optical remote sensing measurements on board a vessel. *Lakes and Reservoirs: Research and Management* 3: 53–66.

Kutser T., Veismann U., Reinart A., Erm A., Herlevi A. & Kallio K. 1999. Field performance of ST-1000 spectrometer in passive optical remote sensing of water bodies. *Proc. Estonian Ac. Sci. Biol. Ecol.* 48: 37–45.

Kutser T., Herlevi A., Kallio K. & Arst H. 2001. A hyperspectral model for interpretation of passive optical remote sensing data. *Sci. Total Environ.* 268: 47–58.

Kutser T., Metsamaa L., Strömbeck N. & Vahtmäe E. 2006. Monitoring cyanobacterial blooms by satellite remote sensing. *Estuarine Coastal and Shelf Science* 67: 303–312.

Lehmusjärvi R. 2004. *Takaisinsironnan todennäköisyys Suomen ja Viron järvissä 1997–2000*. M.Sc. thesis, Division of Geophysics, University of Helsinki.

Leppäranta M. 1995. Optics and heat budget in lakes. *Report Series in Geophysics* 32: 19–27.

Leppäranta M. & Kosloff P. 2000. The thickness and structure of Lake Pääjärvi ice. *Geophysica* 36: 233–248.

Leppäranta M., Tikkanen M. & Shemeikka P. 1998a. Observations of ice and its sediments on the Baltic coast. *Nordic Hydrology* 29: 199–220.

Leppäranta M., Tikkanen M., Shemeikka P. & Virkanen J. 1998b. Observations of ice and its impurities in Finnish lakes. In: Lemmelä R. (ed.), *Proc. 2nd Internat. Conf. Climate and Water, Espoo, Finland, 17–20 August 1998*, vol. 2, Helsinki University of Technology, Espoo, pp. 897–905.

Leppäranta M., Arst H. & Rasmus K. 1999. Passive optical remote sensing of natural water bodies. *Report Series in Geophysics* 41: 4–25.

Leppäranta M., Reinart A., Erm A., Arst H., Hussainov M. & Sipelgas L. 2001. Investigation of ice optical properties in fresh and brackish water bodies. In: Kajander J. & Kuusisto E. (eds.), *Proc. 13th Internat. Symp. Northern Research Basins, Saariselkä and Murmansk 19–24 August 2001*, Finnish Environment Center, Helsinki, pp. 21–29.

Leppäranta M., Reinart A., Erm A., Arst H., Hussainov M. & Sipelgas L. 2003a. Investigation of ice and water properties and under-ice light field in fresh and brackish water bodies. *Nordic Hydrology* 34: 245–266.

Leppäranta M., Tikkanen M. & Virkanen J. 2003b. Observations of ice impurities in some Finnish lakes. *Proc. Estonian Acad. Sci. Chemistry* 52: 59–75.

Lorenzen C.J. 1967. Determination of chlorophyll and phaeopigments; spectrophotometric equations. *Limnol. Oceanogr.* 12: 343–346.

Maritorena S., Morel A. & Gentili B. 2000. Determination of the fluorescence quantum yield by oceanic phytoplankton in their natural habitat. *Applied Optics* 39: 6725–6737.

Mäekivi S. & Arst H. 1996. Estimation of the concentration of yellow substance in natural waters by beam attenuation coefficient spectra. *Proc. Estonian Acad. Sci. Biol. Ecol.* 6: 108–123.

Nõges P., Nõges T. & Reinart A. 1998. The results of bio-optical measurements in Estonian lakes in 1995–1996. *Report Series in Geophysics* 38: 33–46.

Oceanographical Tables 1975. Gidrometeoizdat, Leningrad [In Russian].

Paavel B., Arst H. & Herlevi A. 2007: Dependence of spectral distribution of inherent optical properties of lake waters on the concentrations of different water constituents. *Nordic Hydrology* 3: 265–285.

Paavel B., Arst H., Reinart A. & Herlevi A. 2006. Model calculations of diffuse attenuation coefficient spectra in lake waters. *Proc. Estonian Acad. Sci. Biol. Ecol.* 55: 61–81.

Palosuo E. 1965. Frozen slush on lake ice. *Geophysica* 9: 131–147.

Preisendorfer R.W. 1961. Application of radiative transfer thery to light measurements in the sea. *Union Geod. Geoph. Inst. Monogr.* 10: 11–29.

Rasmus K., Ehn J., Granskog M., Lindfors A., Pelkonen A., Rasmus S., Leppäranta, M. & Reinart A. 2002. Optical measurements of sea ice in Tvärminne, Gulf of Finland. *Nordic Hydrology* 33: 207–226.

Reinart A. 2000. Underwater light field characteristics in different types of Estonian and Finnish lakes. *Dissertationes Geophysicales Universitatus Tartuensis* 11: 1–194.

Reinart A. & Herlevi A. 1999. Diffuse attenuation coefficient in some Estonian and Finnish lakes. *Proc Estonian Acad. Sci. Biol. Ecol.* 48: 267–283.

Reinart A. & Kutser T. 2006. Comparison of different satellite sensors in detecting cyanobacterial bloom events in the Baltic Sea. *Remote Sensing of Environment* 102: 74–85.

Reinart A., Arst, H., Nõges P. & Nõges T. 1998a. Underwater light field in PAR region of the spectrum in some Estonian and Finnish lakes in 1995–1996. *Report Series in Geophysics* 38: 23–33.

Reinart A., Arst H., Blanco-Sequerios A. & Herlevi A. 1998b. Relation between underwater irradiance and quantum irradiance in dependence on water transparency at different depths in the water bodies. *J. Geophys. Res.* 103(C4): 7749–7752.

Reinart A., Arst H., Nõges P. & Nõges T. 2000. Comparison of euphotic layer criteria in lakes. *Geophysica* 36: 141–159.

Reinart A., Arst H., Erm A., Trei T. & Hussainov M. 2001. Optical and biological properties of Lake Ülemiste, a water reservoir of the city of Tallinn II: Light climate in Lake Ülemiste. *Lakes and Reservoirs: Research and Management* 6: 75–84.

Reinart A., Herlevi A., Arst H. & Sipelgas L. 2003. Preliminary optical classification of lakes and coastal waters in Estonia and south Finland. *J. Sea Res.* 49: 357–366.

Reinart A., Arst H. & Pierson D. 2005. Optical properties and light climate in Lake Verevi. *Hydrobiologia* 44: 41–49.

Sipelgas L. 2002. *Erinevat tüüpi bio-optiliste karakteristikute muutlikkus Läänemere regioonis*. M.Sc. thesis, University of Educational Sciences of Tallinn.

Sipelgas L., Arst H., Kallio K., Erm A., Oja P. & Soomere T. 2003. Optical properties of dissolved organic matter in Finnish and Estonian lakes. *Nordic Hydrology* 34: 361–386

Virta J. & Herlevi A. 1997. Correcting errors associated with underwater spectral irradiance measurements. *Proc Estonian Acad. Sci. Biol. Ecol.* 48: 143–148.

Wang C., Shirasawa K., Leppäranta M., Ishikawa M., Huttunen O. & Takatsuka T. 2005. Solar radiation and ice heat budget during winter 2002–2003 in Lake Pääjärvi, Finland. *Verh. Internat. Verein Limnol.* 29: 414–417.

Wang K., Leppäranta M. & Reinart A. 2006. Modeling ice dynamics in Lake Peipsi. *Verh. Internat. Verein Limnol.* 29: 1443–1446.

Zaneveld J.R.V., Kitchen J.C., Bricaud A. & Moore C. 1992. Analysis of in situ spectral absorption meter data. *Ocean Optics* 11: 187–200.